PHYSICAL REVIEW D VOLUME 21, NUMBER 1 1 JANUARY 1980

Basic processes and formalism for the hadronic production of three large-p_T jets

Thomas Gottschalk and Dennis Sivers
High Energy Physics Division, Argonne National Laboratory, Argonne, Illinois 60439
(Received 1 June 1979, revised manuscript received 8 August 1979)

We evaluate those processes in perturbative quantum chromodynamics which can lead to the production of three high-p_T jets in hadron-hadron collisions. A formalism is proposed which incorporates event vetos to separate hard-scattering jets from spectator jets. These vetos modify the scaling violations of the initial parton distribution functions. A simple estimate indicates that the three-jet fraction in high-p_T hadron processes may be up to four times larger than the corresponding three-jet fraction in e^+e^- annihilation.

I. INTRODUCTION

We now have excellent reason to believe that it is possible to use quantum-chromodynamics (QCD) perturbation theory to discuss cross sections for the production of hadrons or hadronic jets at large transverse momentum. There are two components to the reasoning behind this belief:

First, the property of asymptotic freedom insures that the running coupling in QCD becomes small in kinematic regimes characterized by large momentum transfers between fundamental constituents.[1,2] This means that we should be able to calculate an approximation to these large-momentum-transfer processes using the perturbation expansion.

Second, it has now been shown possible to factorize perturbation-theory diagrams[3-5] so that the leading soft or collinear (infrared) divergences can be isolated and, hence, absorbed into unknown distribution functions or decay functions. These unknown functions should have a mild (logarithmic) dependence on the momenta of the hard internal subprocess. The distribution functions should be approximately universal (subject to the uncertainty of higher-order or nonperturbative effects) so that they can be used in many different processes.

These two features indicate that it is sensible to organize the calculation of large-p_T hadron production in the framework of the parton or hard-scattering model as long as one uses scale-violating quark and gluon distribution functions and the appropriate form of the perturbation series for the internal processes. They are not sufficient to guarantee that we can calculate cross sections to arbitrary precision. For example, there may be nonperturbative effects of unknown magnitude which destroy the assumed factorization properties of the hard-scattering model.[6] Or else the perturbation series may be slowly converging so that, in kinematic regimes where α_s is not truly miniscule, results are changed significantly by high-order corrections.[7]

In this respect, it is important that the formal demonstrations of the consistency of the general hard-scattering model in Refs. 3–5 have been supplemented by specific phenomenological studies of high-p_T production by Feynman, Field, and Fox,[8] by Owens and collaborators[9] and by Contogouris, Gaskell, and Papadopoulos.[10] The overall agreement of these calculations with each other and with data is reassuring. They begin to disagree at low values of transverse momentum, where the exact form of k_T fluctuations in the parton distribution functions or the contributions of semicoherent constituent-interchange-model (CIM) processes can be important.[11]

The calculations of Refs. 8–10 all represent correct phenomenological applications of QCD within the leading-logarithm approximation for higher-order corrections. In order to improve our understanding of high-p_T processes, it is obviously important to do calculations which include higher-order corrections in some manner other than the leading-logarithm approximation. This can be difficult. To go beyond the leading-logarithm calculation for the inclusive single-particle cross section, one needs to handle simultaneously a number of effects including (1) nonleading corrections to $\alpha_s(p_T^2)$, the effective coupling in the hard-scattering subprocesses,[12] (2) nonleading corrections to the scaling violations of the quark and gluon distribution functions and decay functions,[13] (3) higher-order corrections to cross sections for the fundamental $2\to2$ processes (virtual loop diagrams), and (4) the contribution of $2\to3$ and $2\to4$ subprocesses in the hard-scattering expansion.

We can, however, decouple the problem of the production processes [(4) above] from the other corrections by defining experimental observables which are preferentially sensitive to them. There are many possible ways of doing this. We will discuss the problem here in terms of "quasiexclusive" jet cross sections in which almost all of the energy in the initial hadron-hadron collisions is

detected either in two jets directed along the initial beam and target directions or in some central region in the c.m. system which contains two, three, four, ... "high-p_T" jets. The purpose of the approach is to define an experimental setup as similar as possible to that used for the analysis of multijet events in e^+e^- annihilation.

The analogy with e^+e^- annihilations is important. De Rújula, Ellis, Floratos, and Gaillard[14] originally performed detailed calculations which showed how multijet events in e^+e^- annihilations could be identified and used to test the underlying perturbation theory. Since that time there have been several other analyses which identify observables sensitive to multijet events in e^+e^- annihilations that can be used to provide nontrivial tests of QCD perturbation theory.[15,16] It would be desirable to apply similar analyses to high-p_T jets produced in hadron-hadron collisions.

There are solid experimental reasons to seek data on multijet events in hadron-hadron collisions in addition to e^+e^- annihilation. The high flux proposed for future hadron-hadron colliding-beam facilities should make it practical to get many more multijet events in high-p_T experiments than possible in e^+e^- machines. This is important since, because of nonperturbative confinement effects, few events are expected to be clean. Measurements which involve finding special axes and sampling techniques will benefit from the added statistics.

In addition, there will be less contamination in pp collisions from events containing either a heavy quark or a τ lepton than would be possible in e^+e^- annihilation. These events are, of course, interesting in their own right, but they can complicate the study of gluon and light-quark jets.

Balanced against the advantages of hadron-hadron collisions for jet production, we must consider the following disadvantages. First, we face the necessity of dealing with the jets of "spectator" partons traveling approximately along the directions of the initial hadrons. What we term "three-high-p_T-jet" events are, in fact, five-jet events if we count the low-p_T particles produced in typical hadron collisions. We shall see, in Sec. II, how this complicates the kinematics. Secondly, there are many more fundamental $2 \to 3$ reactions which must be considered in hadron-hadron collisions. In e^+e^- annihilation, the $O(\alpha_s)$ corrections to the dominant two-jet process can be obtained by looking at $e^+e^- \to q\bar{q}V$.[17] In high-p_T hadron-hadron collisions we must include many $2 \to 2$ processes ($qq \to qq$, $qV \to qV$, $VV \to VV$, etc.) and many more $2 \to 3$ processes ($qq \to qqV$, $qV \to qVV$, $qV \to q\bar{q}q$, etc.), each with its own distinctive features. These must be averaged in order to get observables involving hadrons.

In this paper we would like to discuss the formalism of calculating quasiexclusive jet cross sections in the modified parton model. We discuss the kinematic criteria useful for separating high-p_T events into classes with two, three, or more jets. We give the calculations to lowest order in perturbation theory for the fundamental $2 \to 3$ processes of QCD involving quarks and gluons. With the appropriate interpretation of the observables this will give the three-jet cross section asymptotically within logarithmic accuracy.

The production of three high-p_T jets has been discussed previously by Combridge[18] in the quark-fusion model and also by Kripfganz and Schiller[19] and by Maxwell[20] in the framework of perturbative QCD. Since the basic observables discussed in this paper are different from those of the above authors, we give some of the details and motivation behind our approach.

II. HARD-SCATTERING FORMALISM AND KINEMATICS

The details of the formalism for the hard-scattering model depend on the definitions of the cross sections to be measured. We shall be interested here in the cross sections for the (approximately) exclusive production of high-p_T jets in hadron-hadron collisions. The reason for our approach is the growing belief that jets are the "dressed" quanta of the perturbation theory and the assumption that we can use calculated jet cross sections to define hadronic observables insensitive to questions of how jets materialize as hadrons in much the same way as has been done in e^+e^- annihilations.[15-17] An exclusive observable then has direct contact with the underlying dynamics.

A. Veto-restricted cross sections

Following the work of Sterman[21] and Tiktopoulos,[22] we suggest that the following criteria can be used to specify consistent and useful cross sections. We define cross sections for the large-p_T production of hadrons such that an idealized detector vetos an event if any particle or group of particles deposits more than a small fraction of the available c.m. energy ($E^{\text{c.m.}} \gtrsim \epsilon\sqrt{s}$) outside of the acceptable kinematic region sketched in Fig. 1. (We will, for simplicity, usually define our experimental criteria in terms of c.m. energies and angles. As emphasized by Furmanski[23] a boost-invariant set of criteria would require us to use rapidities. Since we will always calculate Lorentz-invariant quantities up to the imposition of the veto requirement, we can restore Lorentz invariance by giving a boost-invariant veto criterion.) By vetoing events with large en-

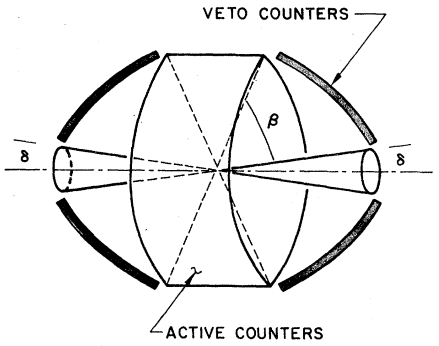

FIG. 1. Figure which specifies configuration for quasiexclusive jet cross sections. Events are vetoed if particles deposit energy $>E_0$ ($E_0/\sqrt{s}>\epsilon$) in the region of c.m. angle $\beta>\theta_{\text{forbid}}>\delta$ or $\beta>(\pi-\theta_{\text{forbid}})>\delta$, and the forward and backward cones contain remnants of the beam and target particles. Active counters cover the central and measure energy E_T which can be made from two, three, ... "large-p_T" jets. No counters need be along the beam and target directions.

ergy deposited in the region $\theta_{\text{c.m.}}\in(\delta,\beta)$ or $(\pi-\beta,\pi-\delta)$ in this manner, we have defined a quasiexclusive configuration where most of the energy is carried by either the two jets along the initial beam and target direction or by one, two, three,... "high-p_T" jets in the central region. If we choose the energy detected in the central region to be large, we can eliminate (by transverse momentum conservation) the possibility that it is carried by one quantum. We can therefore guarantee that we are counting events which are the result either of a hard 2-2 scattering among constituents or of a hard jet-production process such as $qq\to qqV$ or $qV\to qVV$ in a manner similar to that originally advocated by Bjorken.[24] We will be able to find criteria for separating events in the central region into categories such as two jets or three jets by using analogs of observables such as thrust defined for e^+e^- annihilation events.

In the usual formulation of the hard-scattering model[25] it is assumed that large-p_T events are dominated by hard $2\to2$ subprocesses. To understand this assumption in a scale-invariant theory, we can use familiar dimensional-counting arguments. An internal process, where two energetic constituents collide to produce n large-p_T jets ($h_ah_b\to j_1j_2\cdots j_n$), gives rise to a cross section

$$E_1\cdots E_{(n-1)}\frac{d\sigma}{d^3p_1\cdots d^3p_{(n-1)}}\propto s^{-n}H_n(p_i\cdot p_j/s) \tag{2.1}$$

(modulo factors involving logarithms) in a kinematic region where all invariants $p_i\cdot p_j$ become large and proportional to s. The contribution from a *finite region* of phase space to the inclusive single-particle production cross section behaves as

$$E\frac{d\sigma^{(n)}}{d^3p}\bigg|_{\text{finite}}\propto s^{-n}H_n(x_T=2p_T/\sqrt{s},\theta), \tag{2.2}$$

(modulo logs) and, hence, the single-particle production appears to be dominated by $2\to2$ subprocesses. However, what really happens is much more subtle. Notice that if we were to naively integrate the cross section in Eq. (2.1) over *all phase space*, we would necessarily enter regions where the perturbative calculation has either soft divergences ($p_i\to0$) or collinear divergences ($p_i\cdot p_j\to0$). These divergences must be regularized in some manner such that we get finite results when we sum over all physically degenerate states. These procedures are familiar in QED, and there have been several recent discussions of their applications to QCD calculations.[3-5] It can be shown that, with logarithmic accuracy, the divergences can be absorbed into scaling-violating distributions or into the final-state-jet observables such that the $2\to2$ configuration still dominates if we interpret our quanta to be jets of finite angular resolution. The dominance is, however, only logarithmic. That is, if we integrate (2.1) "hard" multibody phase space where all invariants are large, $p_i\cdot p_j>\epsilon s$, and jets can, in principle, be isolated, we obtain a contribution to the single-particle inclusive distribution which has the same power behavior as the $2\to2$ contribution but fewer powers of logarithms. The separation of these nonleading contributions from other "corrections" to the single-particle inclusive distribution depends on conventions, i.e., just how we choose to absorb the contributions from the "soft" regions into the distribution functions. We will not address this question here. Instead, we turn to the calculation of these quasiexclusive jet cross sections which are directly related to the existence of $2\to3$ processes.

B. General kinematic constraints

The experimental configuration proposed above provides constraints on the various kinematic observables which appear in the formulation of the hard-scattering model. Because of the veto requirement, the quark and gluon distribution functions which enter into the calculation are not identical to those in the usual inclusive formulation. We denote $G^{\delta}_{a/A}(x,\vec{k}_T,\ln P^2)$ as the distribution function for a parton a to carry fraction x of hadron A's longitudinal momentum P subject to the veto requirement that no hadrons deposit a large amount of energy outside of an angle δ from the direction of P. We will discuss these distribution

functions in more detail in Appendix A. Here we will just summarize some of their properties. The first constraint we will consider is that on the transverse momentum of the initial partons. We should have approximately

$$k_T \lesssim \max[k_T^0, P(1-x)\sin\delta], \tag{2.3}$$

where $p_{aL} = xP$ and k_T^0 is some momentum associated with the scale of nonperturbative effects in QCD. The constraint (2.3) is necessary in order that the unscattered remnants of hadron A are not directed outside the allowed cone for the initial hadron jet in Fig. 1.

Because the angular gap in the experimental setup removes significant interference terms between initial- and final-state jets, we can justify the use of the probabilistic hard-scattering formula for the production of n distinct high-p_T jets in the central detector,

$$\left.\frac{d\sigma(AB\to 12\cdots nX)}{\left(\frac{d^3p_1}{2E_1}\right)\left(\frac{d^3p_2}{2E_2}\right)\cdots\left(\frac{d^3p_n}{2E_n}\right)}\right|_{\delta_1\delta_2\beta_1\beta_2}^{\epsilon} \cong \left(\frac{1}{2\pi}\right)^{3n-4} \sum_{ab\to 12\cdots nX} \int d^2k_{Ta}dx_a G_{a/A}^{\delta_1}(x, k_{Ta}, \ln P^2) d^2k_{Tb}dx_b G_{b/B}^{\delta_2}(x_b, k_{Tb}, \ln P^2)$$

$$\times \frac{1}{2x_a x_b s}\left|\hat{M}_{ab\to j_1\cdots j_n X}(\hat{p}_1\cdot\hat{p}_j\cdots)\right|^2_{\beta_1\beta_2} \times \delta^{(4)}\left(p_a+p_b-\sum_{j=1}^{n}p_i-p_0\right)\left(\int_{\pm\epsilon\sqrt{s}}\frac{d^4p_0}{(2\pi)^3}\right). \tag{2.4}$$

We have included in (2.4) the integration over unobserved quanta outside of the forward and backward cones as a single "phantom" particle p_0 either in the initial or final state. In order that each of the large-p_T jets be observable we shall require

$$2x_T = E_T/\sqrt{s} \gtrsim n\cdot\epsilon, \tag{2.5}$$

where E_T is the c.m. energy detected in the central, active detector. We should also impose the constraint

$$E_T/\sqrt{s} \lesssim 1-2\epsilon, \tag{2.6}$$

which guarantees that the forward and backward "spectator" jets can exist and that we are not trying artificially to discuss coherent processes within the framework of an incoherent, parton-model formalism. Other approaches based on counting rules, factorization, etc., of various coherent (constituent-interchange model) processes seem more appropriate to the regime of high-x_T events. These approaches are discussed elsewhere.[11] Expressions (2.5) and (2.6) express the fact that we want each of the jets to have more c.m. energy than $\epsilon\sqrt{s}$ and that it is not possible with finite resolution to arbitrarily subdivide the system indefinitely. With, for example, $\epsilon = 0.1$, (2.5) and (2.6) tell us it is meaningful to try to separate two-jet and three-jet events for

$$E_T/\sqrt{s} \in (0.3,\ 0.8), \tag{2.7}$$

CERN ISR $\sqrt{s} = 60$ GeV, $E_T \in (18, 48)$ GeV, (2.8)

(proposed) ISABELLE $\sqrt{s} = 400$ GeV, $E_T \in (120, 320)$ GeV. (2.9)

By changing ϵ, it is possible to expand or contract this region. Note that we are assuming a hypothetical detector which in both the active and veto regions are equally sensitive to neutral and charged particles. If we consider the central detector as a single entity, the cross section for it to detect energy $E_T(x_T \neq 0, 1)$ is finite and calculable in the hard-scattering model. For this reason we do not need to specify the energy or angular resolution of each jet separately at this point. These resolution questions will become important when we explicitly try to separate two-jet and three-jet events.

Let us consider briefly some of the other constraints implicit in Eq. (2.4). In the hard scattering depicted in Fig. 2, constituent a is carried off mass shell by an amount[25]

$$(p_a^2 - m_a^2) \cong x_a\left(m_A^2 - \frac{k_{Ta}^2 + m_{A\bar{a}}^2}{(1-x_a)} - \frac{m_a^2 + k_{Ta}^2}{x_a}\right), \tag{2.10}$$

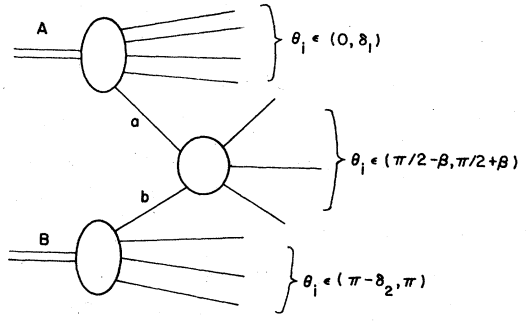

FIG. 2. Hard-scattering-model configuration.

where x_a is the light-cone scaling variable. The veto constraint we introduce restricts both $k_{Ta}{}^2$ as in (2.3) and $m_{A\bar{a}}{}^2$ since the relative k_T of particles in the $A\bar{a}$ cluster must be limited. For simplicity we assume we can neglect the later effect, suppress all intrinsic masses in (2.10), and write using (2.3)

$$(p_a{}^2/P^2) \lesssim (1-x_a)\sin^2\delta + O(m^2/P^2)\,. \tag{2.11}$$

When we calculate in the framework of the hard-scattering model using on-mass-shell parton kinematics for the internal subprocesses we may be making errors proportional to $(p_a{}^2/P^2)_{\max}$. Two simple examples of the kinds of errors possible are instructive. Off-mass-shell gluons can have longitudinal polarization. Cross sections for scattering from these modes will vanish as $p_a{}^2 \to 0$ but we have an uncertainty

$$\frac{\Delta\sigma_L(p_a{}^2,\hat{s},\theta_i)}{\Delta\sigma_T(p_a{}^2,\hat{s},\theta_i)} \approx \left\langle \frac{p_a{}^2}{\hat{s}} \right\rangle_{\text{average}} \lesssim \frac{(1-x_a)\sin^2\delta}{4x_a x_b}\,. \tag{2.12}$$

In the symmetric region where $x_a \cong x_b \cong x_T$,

$$\Delta\sigma_L/\Delta\sigma_T \lesssim \frac{(1-x_T)\sin^2\delta}{4x_T{}^2}\,. \tag{2.13}$$

The exact amount of the error depends on the shape of the k_T distribution and the processes involved. We can see by the form of (2.13) that the main contribution is at small x_T.

In a similar manner, we can consider some purely kinematic uncertainties associated with the hard-scattering model. Using the dimensional-counting rules[26] we can write

$$d\hat{\sigma}_{2\to n} \simeq \hat{s}^{-n} f(\theta_{ik})\,. \tag{2.14}$$

Owing to possible off-shell effects, we have a kinematic uncertainty in the invariant subenergy $\hat{s}$ of the internal process. Using (2.1) this can lead to an uncertainty

$$\frac{\Delta d\hat{\sigma}}{d\hat{\sigma}} \cong -n\left(\frac{\Delta\hat{s}}{\hat{s}}\right) \lesssim \frac{-n}{2}\frac{\sin^2\delta}{x_a x_b}\left[\frac{x_b}{x_a}(1-x_a)^2 + \frac{x_a}{x_b}(1-x_b)^2 + 2(1-x_a)(1-x_b)\right]$$

$$\lesssim \frac{-n\sin^2\delta}{2x_T{}^2}[4(1-x_T)^2]\,. \tag{2.15}$$

Again, to keep this possible source of error under control, we must stay away from x_T near 0.

The uncertainties we have discussed so far are proportional to $\sin^2\delta$. We should also mention that the scaling violations in the distribution functions $G^{\delta}_{a/A}(x, k_T, \ln P^2)$ should be most conveniently expressed in terms of the variable

$$\xi_\delta = \ln(k_{T\max}{}^2/\Lambda^2) \cong \ln\left(\frac{P^2\sin^2\delta}{\Lambda^2}\right), \tag{2.16}$$

where $\Lambda \cong 0.3$–0.7 GeV governs the scale of the QCD coupling. If we want to require that the scaling violation in these distribution functions be calculable in QCD perturbation theory, we will want the opening angle to be chosen large enough so that $k_{T\max}{}^2/\Lambda^2 \gg 1$. This is discussed further in Appendix A.

Kinematic uncertainties of the type illustrated in (2.15) appear also in inclusive cross sections and have been handled phenomenologically in several ways. One approach is to use specific regularization parameters in the perturbative cross sections to protect IR-sensitive regions in the integrations in (2.4).[8-10] Another approach is to use the off-shell estimate (2.10) with a specific value for $m_{A\bar{a}}{}^2$ as a strict equality together with off-shell generalizations of parton kinematics.[27] The extent to which different assumptions give different answers depends on the distribution functions, but we can get a rough measure of the uncertainty by using (2.15). Of course, to actually resolve these uncertainties one must carefully consider higher-order effects.

C. Final-state identification and the two-jet background

In the preceeding sections we have argued that, with some restrictions on the fractional energy x_T deposited in the central region, the hard-scattering model provides a reliable description of hadronic exclusive multijet production. We can now discuss the classification of events with respect to the jet multiplicity in the central hadronic detector. Several observables sensitive to the jet topology of events in $e^+e^- \to$ hadrons have been proposed.[12-16] To be meaningful calculable in terms of underlying QCD processes, these variables must be insensitive to the parallel decay of any quantum involved. Such variables are then said to be infrared safe.

We shall consider two basic types of these observables.

Thrust. The thrust variables was first suggested by Fahri[28] for $e^+e^- \to$ hadrons and the transverse thrust defined as

$$T_T = 4\max d_T(\hat{r}) - 1\,, \tag{2.17}$$

where

$$d_T(\hat{r}) = \frac{\sum_j (\hat{r}\cdot\vec{p}_{Tj})\theta(\hat{r}\cdot\vec{p}_{Tj})}{\sum_j |p_{Tj}|}\,,$$

and $\hat{r}$ is a unit vector in the transverse plane, was introduced by Maxwell[20] to describe large-p_T production.

Shape variables. Among the general class of variables which are sensitive to the event shape but which do not depend on maximizing with respect to a specific vector, we can consider the observables

$$H_l = \sum_{ij} \frac{|\vec{p}_{Ti}||\vec{p}_{Tj}|}{\hat{s}} P_l(\cos(\phi_i - \phi_j)), \tag{2.18}$$

where $\hat{s} = 4E_T{}^2$ and

$$C_l = \left| \sum_i |p_{Ti}| e^{il\phi_i} \right|^2, \tag{2.19}$$

suggested by Fox and Wolfram.[16] In applying the variables (2.17)–(2.19) to hadronic multijet production, we restrict the summations to particles observed in the central region.

For the lowest-order QCD process in electron-positron annihilation $e^+e^- \to q\bar{q}$, the analogous variables have trivial values

$$T(e^+e^- \to q\bar{q}) = 1, \qquad H_l(e^+e^- \to q\bar{q}) = \begin{cases} 0, & \text{odd } l \\ 1, & \text{even } l. \end{cases} \tag{2.20}$$

Empirical studies of the fragmentation of "free" quarks and gluons into physical jets spread these extreme values, but indicate that, for $E_{\text{had}} \gtrsim 15$ GeV, these nonperturbative effects do not completely obscure three-jet events arising from $e^+e^- \to q\bar{q}V$.[14-16]

In hadronic multijet production, the situation is further complicated by the intrinsic inability to completely specify the underlying kinematics. Ideally, the values of thrust and the shape variables should be measured in the c. m. frame of the hard-scattering subprocess. In general, this frame coincides with neither the c. m. frame of the incident hadrons (due to parton transverse momenta) nor the c. m. frame derived from the particle configuration in the central detector (due to possible unobserved hard-scattering participants). To get some feel for these effects of such uncertainties, we examine the kinematics of two-jet events in some detail, interpreting Eqs. (2.17)–(2.19) via measured hadronic c. m. quantities. In the hadron-hadron c. m. system, we write the parton four momenta as

$$\begin{aligned} p_a &= ((x_a{}^2P^2 + m_{Ta}{}^2)^{1/2}, k_{Ta}\sin\phi_a, k_{Ta}\cos\phi_a, x_aP), \\ p_b &= ((x_b{}^2P^2 + m_{Tb}{}^2)^{1/2}, k_{Tb}\sin\phi_b, k_{Tb}\cos\phi_b, -x_bP), \\ p_1 &= z_1P(1, \sin\theta_1\sin\phi_1, \sin\theta_1\cos\phi_1, \cos\theta_1), \\ p_2 &= z_2P(1, \sin\theta_2\sin\phi_2, \sin\theta_2\cos\phi_2, \cos\theta_2), \\ p_0 &= z_0P(r, \sin\theta_0\sin\phi_0, \sin\theta_0\cos\phi_0, \cos\theta_0), \end{aligned} \tag{2.21}$$

where p_0 denotes a possible unobserved parton jet. We restrict

$$\begin{aligned} &|rz_0| < \epsilon, \\ &z_1, z_2 > \epsilon. \end{aligned} \tag{2.22}$$

For the observed two-jet parton state, the measured thrust value is (assuming complete detection)

$$T_T(\text{parton}) = 2\max\{z_{1T}, z_{2T}\}/(z_{1T} + z_{2T}), \tag{2.23}$$

where $z_{iT} = z_i \sin\theta_i$. Because of the possible undetected jet p_0 and the transverse momentum of the initial state, we do not, in general, have $z_1 = z_2$, so that

$$T_T(\text{parton}) > 1, \tag{2.24}$$

and we expect a shift to larger values of thrust by an amount

$$\Delta T_T \lesssim 2\sin\delta\left(\frac{1 - z_1}{z_1}\right) + \frac{\epsilon}{2z_1}. \tag{2.25}$$

This is in the opposite direction from the shift in thrust of two-jet events due to the decay of the jets into physical hadrons. Small measured thrusts in large-p_T hadron-hadron collisions therefore reliably signal multijet final states.

The effects of incomplete initial/final-state information are more troublesome for the shape variables. Let us first consider the azimuthal relationship between the jets. This was first identified by Bjorken[24] as a signature for two-jet processes. Define a transverse frame so that $\sin\phi_1 = 0$. From transverse momentum conservation and the constraint (2.3), we have

$$|\sin\phi_2| < \frac{(2 - z_{1T} - z_{2T})\sin\delta + \epsilon}{z_{2T}},$$

so that ϕ_2 is centered around π with smearing which is limited by our choice of δ, ϵ. The exact amount of smearing within the allowed range depends on the distribution functions. We can see, however, that this smearing due to missing transverse momentum will affect the shape variables in the same way as the hadronic decay or "confinement" effects. For example, since $\cos(\phi_1 - \phi_2) < 1$, $H_2 < 1$. Since these effects can be limited, it still makes sense to use shape variables to separate two-jet events, but the separation may not be as clearcut as that obtained from a thrust cut.

Another important kinematic effect arises if we attempt to measure the scaling variables x_a, x_b of the initial partons. The δ-function constraint for $p_a + p_b \to p_1 + p_2 + p_0$ implies

$$x_a \simeq z_1\left(\frac{1 + \cos\theta_1}{2}\right) + z_2\left(\frac{1 + \cos\theta_2}{2}\right) + z_0\left(\frac{1 + \cos\theta_0}{2}\right) - \frac{1}{2}\frac{m_{Ta}{}^2}{x_aP^2}. \tag{2.26}$$

If we denote the "observed" value by

$$x_a^{(1)} = z_1\left(\frac{1+\cos\theta_1}{2}\right) + z_2\left(\frac{1+\cos\theta_2}{2}\right), \tag{2.27}$$

then, we have to smear $G^{\delta}(x_a, k_{Ta}, \ln P^2)$ near $x_a = x_a^{(1)}$ by an amount

$$\delta x_a \lesssim \epsilon + \left(\frac{1-x_a}{2}\right)\sin^2\delta\,. \tag{2.28}$$

Only if ϵ and $\sin^2\delta$ are small is x_a well determined; for steeply falling parton distributions, such discrepancies can have large effects. This structure function dependence can be partially eliminated by considering the ratio of various multijet cross sections at fixed observed x_T, as discussed in the next section.[19]

D. Elementary $2 \to 3$ kinematics

Given our "experimental" definition for multijet cross sections in Eq. (2.4), the underlying hard-scattering process for three-jet production is potentially a $2 \to 4$ process

$$p_a + p_b \to p_1 + p_2 + p_3 + p_0\,, \tag{2.29}$$

where p_0 again represents a possible unobserved jet. In the c. m. system of the colliding hadrons, we can parametrize the involved four momenta as

$$\begin{aligned}
p_a &= ((x_a{}^2P^2 + m_{Ta}{}^2)^{1/2},\ k_{Ta}\sin\phi_a,\ k_{Ta}\cos\phi_a,\ x_aP)\,,\\
p_b &= ((x_b{}^2P^2 + m_{Tb}{}^2)^{1/2},\ k_{Tb}\sin\phi_b,\ k_{Tb}\cos\phi_b,\ -x_bP)\,,\\
p_1 &= z_1P(1,\ \sin\theta_1\sin\phi_1,\ \sin\theta_1\cos\phi_1,\ \cos\theta_1)\,,\\
p_2 &= z_2P(1,\ \sin\theta_2,\ \sin\phi_2,\ \sin\theta_2\cos\phi_2,\ \cos\theta_2)\,,\\
p_3 &= z_3P(1,\ \sin\theta_3\sin\phi_3,\ \sin\theta_3\cos\phi_3,\ \cos\theta_3)\,,\\
p_0 &= z_0P(r,\ \sin\theta_0\sin\phi_0,\ \sin\theta_0\cos\phi_0,\ \cos\theta_0)\,.
\end{aligned} \tag{2.30}$$

In complete generality, this configuration is described by eleven Lorentz scalars p_a^2, p_b^2, p_0^2 and the eight independent dot products $p_i \cdot p_j$. To simplify the analysis, we shall first work only to zeroth order in δ, ϵ [i.e., setting z_0, k_{Ta}, $k_{Tb} \to 0$ in Eq. (2.30)]. We shall discuss briefly the effects of nonzero δ, ϵ at the end of this section.

Neglecting ϵ, δ in the kinematics, we can rewrite the three-jet production cross section as

$$\begin{aligned}
&d\sigma(AB \to 3\text{ jet}, X)\\
&\simeq \sum_{a,b=1}^{23} \int dx_a dx_b \tilde{G}^{\delta}_{a/A}(x_a)\tilde{G}^{\delta}_{b/B}(x_b)\\
&\qquad \times \frac{1}{2x_ax_bS}\langle |M_{ab\to 123}|^2\rangle d^3P_{\mathrm{LI}}\,,
\end{aligned} \tag{2.31}$$

where

$$\tilde{G}^{\delta}(x) \equiv \int d^2k_T G^{\delta}(x, k_T)\,, \tag{2.32}$$

and

$$d^3P_{\mathrm{LI}} \equiv (2\pi)^{-5}\delta^{(4)}(p_a + p_b - p_1 - p_2 - p_3)\prod_{j=1}^{3}\frac{d^3p_j}{2E_j}\,. \tag{2.33}$$

We expand this Lorentz-invariant (LI) phase-space element in the c. m. system of the colliding partons. First we define

$$\begin{aligned}
\hat{s} &\equiv (p_a + p_b)^2 \simeq x_ax_bs\,,\\
\hat{x}_j &\equiv 2E_j^*/\sqrt{\hat{s}}\,,
\end{aligned} \tag{2.34}$$

where E_j^* is the energy of jet j in the parton-parton c. m. frame, and

$$\hat{x}_1 + \hat{x}_2 + \hat{x}_3 = 2\,. \tag{2.35}$$

We also define the normal to the final state plane

$$\hat{n} \equiv (\vec{p}_1^{\,*} \times \vec{p}_2^{\,*})/|\vec{p}_1^{\,*} \times \vec{p}_2^{\,*}|\,. \tag{2.36}$$

The five independent scalars defining the kinematics are taken to be $\hat{s}, \hat{x}_1, \hat{x}_2, \phi_n, \theta_n$, where ϕ_n and θ_n orient $\hat{n}$ with respect to $\vec{p}_a$. Then

$$d^3P_{\mathrm{LI}} = \frac{1}{(2\pi)^4}\frac{\hat{s}}{32}d\hat{x}_1 d\hat{x}_2 d\phi_n d(\cos\theta_n)\,. \tag{2.37}$$

Using a coordinate frame with $\hat{z} = \hat{n}$, $\hat{x} = \hat{p}_1$, the c. m. momenta can be written as

$$\begin{aligned}
p_a &= (\sqrt{\hat{s}}/2)(1,\ \sin\theta_n\cos\phi_n,\ \sin\theta_n\sin\phi_n,\ \cos\theta_n)\,,\\
p_b &= (\sqrt{\hat{s}}/2)(1,\ -\sin\theta_n\cos\phi_n,\ -\sin\theta_n\sin\phi_n,\ -\cos\theta_n)\,,\\
p_1 &= (\hat{x}_1\sqrt{\hat{s}}/2)(1,\ 1,\ 0,\ 0)\,,\\
p_2 &= (\hat{x}_2\sqrt{\hat{s}}/2)(1,\ \cos\theta_{12},\ \sin\theta_{12},\ 0)\,,\\
p_3 &= (\hat{x}_3\sqrt{\hat{s}}/2)(1,\ \cos\theta_{13},\ -\sin\theta_{13},\ 0)\,,
\end{aligned} \tag{2.38}$$

where

$$\cos\theta_{ij} = 1 - 2(\hat{x}_i + \hat{x}_j - 1)/(\hat{x}_i\hat{x}_j)\,. \tag{2.39}$$

The description of three-jet production simplifies further if we take $\beta \to \pi/2$ in Fig. 1. In this limit

$$\begin{aligned}
&x_a \to x_b \equiv x_T\,,\\
&\cos\theta_n \to \pm 1\,.
\end{aligned} \tag{2.40}$$

With $\sin\beta, \epsilon, \delta$ all zero, the scalar products for the $2 \to 3$ process are

$$\begin{aligned}
&\hat{s} = 2p_a \cdot p_b = x_T{}^2 s\,,\\
&4p_a \cdot p_1 \cong 4p_b \cdot p_1 \cong \hat{s}\hat{x}_1\,,\\
&4p_a \cdot p_2 \cong 4p_b \cdot p_2 \cong \hat{s}\hat{x}_2\,,\\
&4p_a \cdot p_3 \cong 4p_b \cdot p_3 \cong \hat{s}\hat{x}_3\,,\\
&2p_1 \cdot p_2 \cong \hat{s}(1 - \hat{x}_3)\,,\\
&2p_2 \cdot p_3 \cong \hat{s}(1 - \hat{x}_1)\,,\\
&2p_1 \cdot p_3 \cong \hat{s}(1 - \hat{x}_2)\,.
\end{aligned} \tag{2.41}$$

The azimuth ϕ_n thus decouples, so that

$$d^3P_{\rm LI}\big|_{\cos^2\theta_n=1}=\frac{\hat{s}}{16(2\pi)^3}d\hat{x}_1 d\hat{x}_2\,. \tag{2.42}$$

It is instructive to investigate the final-state topology using a Dalitz plot in the scaled energies $\hat{x}_j$, as shown in Fig. 3. Using Eqs. (2.35) and (2.39), each point in the physical region is paired with a unique event geometry. In the case where we don't measure the flavor or color of the jets, the physical cross section is obtained by summing over the six distinct orderings of the lengths of the momenta p_1, p_2, p_3.

Along the boundaries of the plot, the nominal three-jet configurations are indistinguishable from two-jet systems in which one of the quanta subsequently undergoes parallel decay. As emphasized in Ref. 3, this parallel propagation can occur on an arbitrarily large time scale; such processes are not expected to be describable to perturbative QCD. The inapplicability of perturbation theory is evident in the canonical $(1-\hat{x}_j)^{-1}$ singularities of the corresponding squared matrix elements.

Perturbative description of three-jet production must be restricted to configurations away from the Dalitz plot boundaries. This is easily accomplished by imposing upper limits on the jet parameters T, H_2 discussed in the preceeding section. For idealized kinematics with massless quanta,

$$T_T(\hat{x}_1,\hat{x}_2,\hat{x}_3)=2\max\{\hat{x}_j\}-1\,,$$
$$H_2(\hat{x}_1,\hat{x}_2,\hat{x}_3)=1-6(1-\hat{x}_1)(1-\hat{x}_2)(1-\hat{x}_3)/\hat{x}_1\hat{x}_2\hat{x}_3\,. \tag{2.43}$$

Both T_T, H_2 attain a maximum value of 1 (identical with the two-jet values) on the plot boundary and decrease to minimum values $T_T=\frac{1}{3}$, $H_2=\frac{1}{4}$ at the plot's center $x_j=\frac{2}{3}$. Contours of constant thrust are triangles concentric with the plot boundary. Those for H_2 are qualitatively similar.

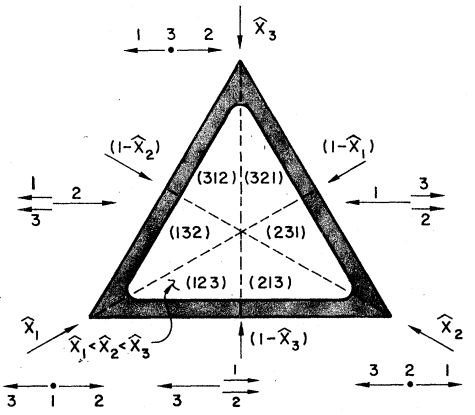

FIG. 3. Dalitz plot for $2\to3$ processes. Collinear configurations of momenta occur on the boundaries as shown. The six regions corresponding to the distinct orderings of x's are also shown.

The effects of the imprecise kinematics on the three-body final states are, in general, complicated. From (2.30) we can see that measurement of p_1, p_2, and p_3 does not completely determine p_a and p_b so that dot products involving both initial and final states are uncertain by amounts which depend on δ, ϵ.

Since $(\vec{p}_{1T}+\vec{p}_{2T}+\vec{p}_{3T})\neq 0$, we can see that transverse thrust can be displaced from the estimate (2.43) by an amount similar to the $2\to2$ case (2.25), but now this displacement can be either positive or negative depending on whether the projection of $p_T^{\max}$ along the β-body motion is positive or negative. Since the distributions in thrust and H_2 for the $2\to3$ processes are increasing as we increase T_T and H near the two-jet boundaries, the overall effect of the uncertain kinematics and of the decay of the jets into hadrons will be to degrade the three-jet values.

III. EVALUATING MATRIX ELEMENTS

In order to use the hard-scattering model discussed in Sec. II for calculating jet cross sections, we need the mean-squared matrix elements for the fundamental $2\to3$ processes in QCD as functions of their kinematic invariants. We now give the calculation of these processes to lowest nontrivial order in the QCD perturbation expansion. Because we will be calculating a large number of processes related by crossing, we will express our results in terms of "cuttings" of diagrams with no external legs.

A. Evaluation of cut QCD diagrams

We summarize here our prescription for calculating the cut diagrams used in evaluating the spin and color summed squared matrix elements for QCD processes. The metric convention is that of Bjorken and Drell.[29] We take all particles to be massless and use spinor normalization $\bar{u}u=2m$.

The rules for vertices and propagators are given in Fig. 4. The tensors appearing in the three-gluon and four-gluon vertices are defined by

$$V^{\alpha\beta\gamma}(p_a,p_b,p_c)\equiv(p_a-p_b)^\gamma g^{\alpha\beta}+(p_b-p_c)^\alpha g^{\beta\gamma}+(p_c-p_a)^\beta g^{\gamma\alpha}\,, \tag{3.1}$$

$$K(\alpha\beta;\gamma\delta)\equiv(g^{\alpha\gamma}g^{\beta\delta}-g^{\alpha\delta}g^{\beta\gamma})\,. \tag{3.2}$$

$T^a=\frac{1}{2}\lambda^a$ and f^{abc} are the usual color matrices and structure constants as discussed in Ref. 30.

The basic procedure for evaluating the cut diagrams is the following.

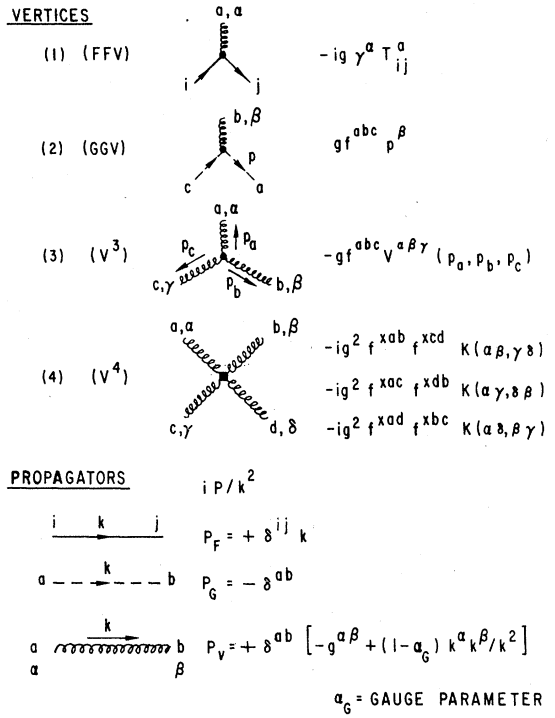

FIG. 4. Feynman rules for QCD perturbation theory.

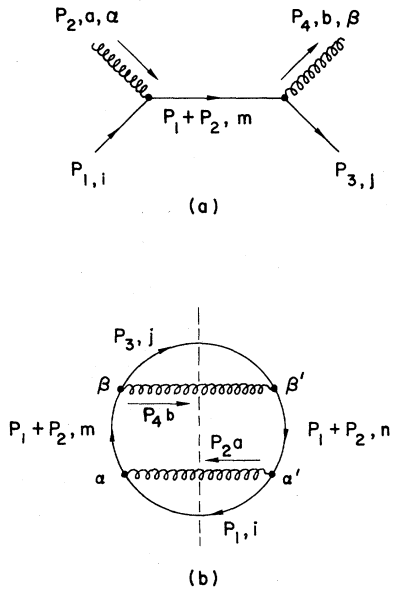

FIG. 5. Squared s-channel contribution to quark-gluon scattering evaluated directly from the corresponding cut diagram.

(i) Using the rules from Fig. 1, construct the expression for the corresponding Feynman diagram.

(ii) Remove the factors i/k^2 for each cut propagator (also ignore loop integrations for cut loops).

(iii) Multiply the resulting expression by -1.

Rule (iii) is easily understood. Unitarity (on which our approach can be based) is formulated in terms of the T matrix, which differs by a factor of i from the S matrix (on which the rules of Fig. 1 are based). The corresponding factor of $(i)^2$ is rule (iii). Note that there is no factor of -1 for cut fermion loops.

As a simple illustration, consider the contribution to $qV \to qV$ scattering arising from the square of the diagram in Fig. 5(a). The corresponding cut cut diagram is shown in Fig. 5(b). The square of the matrix element for Fig. 5(a), summed over colors, spins, is determined from Fig. 5 to be (for $\alpha_G = 1$)

$$\sum_{\substack{\text{colors}\\ \text{spins}}} |M|^2 = (-)(-g^{\alpha\bar{\alpha}})(-g^{\beta\bar{\beta}})\,\mathrm{Tr}(T^aT^bT^bT^a)(-ig)^4\left[\frac{i}{(p_1+p_2)^2}\right]^2 \mathrm{Tr}[\not p_3\gamma^{\beta}(\not p_1+\not p_2)\gamma^{\alpha}\not p_1\gamma^{\bar{\alpha}}(\not p_1+\not p_2)\gamma^{\bar{\beta}}], \tag{3.3}$$

$$= \tfrac{16}{3}g^4\left[\frac{1}{(p_1+p_2)^2}\right]^2 \mathrm{Tr}[\not p_3\gamma^{\beta}(\not p_1+\not p_2)\gamma^{\alpha}\not p_1\gamma^{\alpha}(\not p_1+\not p_2)\gamma^{\beta}], \tag{3.4}$$

where repeated indices are summed.

Given the above rules, we are effectively using a covariant spin sum operator for external gluons:

$$\sum_{\text{spins}} \epsilon^{\alpha}\epsilon^{*\beta} \to -g^{\alpha\beta}+(1-\alpha_G)k^{\alpha}k^{\beta}/k^2 . \tag{3.5}$$

However, in QCD the $k^{\alpha}k^{\beta}$ terms in Eq. (3.5) do not, in general, decouple from the rest of the diagram, so that the basic procedure outlined above above is not gauge invariant. One solution involves replacing the covariant operator in Eq. (3.5) by noncovariant transverse polarization projection operators. This has advantages for certain approximate schemes. For exact expressions, however, we find that such a procedure introduces a great deal of complexity into the calculations. Instead, we remove the unwanted longitudinal polarization components from the spin sums in Eq. (3.5) via Fadeev-Popov ghosts.[31]

Using ghosts, we expand on our previous three steps for evaluating cut diagrams:

(iv) For a given cut diagram, calculate also all

those diagrams obtained by replacing closed gluon loops by ghost loops.

(v) Multiply each ghost diagram's contribution by $(-)^{N_L}$ where N_L is the number of disjoint ghost loops in the diagram.

(vi) Adding all ghost diagram contributions to the original ghostless expression yields the desired physical spin sum.

An example of this procedure is illustrated schematically in Fig. 6. Each cut diagram is evaluated using the basic rules (i)–(iii). The additional minus signs before the two ghost diagrams arise due to the odd number of ghost loops. Note that a given ghost loop can have two directions, leading to two contributions to the physical spin sum.

B. Elementary $2\to3$ processes involving a single gluon

We evaluate here the spin- and color-summed squared matrix elements for the seven distinct $2\to3$ elementary processes involving a single gluon,

$$\text{(F)}\quad q_A(p_1)+q_B(p_2)\to q_A(p_3)+q_B(p_4)+V(p_5),$$

$$\text{(G)}\quad q_A(p_1)+q_A(p_2)\to q_A(p_3)+q_A(p_4)+V(p_5),$$

$$\text{(H)}\quad q_A(k_1)+V(k_2)\to q_A(k_3)+q_B(k_4)+\bar{q}_B(k_5),$$

$$\text{(I)}\quad q_A(k_1)+V(k_2)\to q_A(k_3)+q_A(k_4)+\bar{q}_A(k_5),$$

$$\text{(J)}\quad q_A(k_1)+\bar{q}_B(k_2)\to q_A(k_3)+\bar{q}_B(k_4)+V(k_5),$$

$$\text{(K)}\quad q_A(k_1)+\bar{q}_A(k_2)\to q_A(k_3)+\bar{q}_A(k_4)+V(k_5),$$

$$\text{(L)}\quad q_A(k_1)+\bar{q}_A(k_2)\to \bar{q}_B(k_3)+q_B(k_4)+V(k_5),$$

where A, B represent distinct quark flavors. The charge conjugates of (F)–(I) give four more single gluon processes (which require no new matrix elements).

In evaluating the spin- and color-averaged squared matrix elements, we first introduce two base functions,

$$F(p_1,p_2,p_3,p_4,p_5)\equiv\frac{1}{g^6}\sum_{\text{colors,spins}}|\mathfrak{M}_F|^2,$$
$$G(p_1,p_2,p_3,p_4,p_5)\equiv\frac{1}{g^6}\sum_{\text{colors,spins}}|\mathfrak{M}_G|^2. \tag{3.6}$$

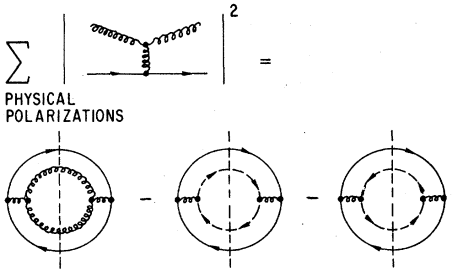

FIG. 6. Schematic illustration of the use of ghosts to remove contributions from longitudinal gluon polarizations.

The corresponding functions for the remaining processes are obtained from F and G by various crossings. For example, $\mathfrak{M}_H$ is obtained from $\mathfrak{M}_F$ by the substitutions

$$\begin{aligned}&u(p_2)\to v(k_5),\\ &p_2\to -k_5,\\ &p_5\to -k_2,\\ &\epsilon_\mu^*\to\epsilon_\mu,\\ &p_1,p_3,p_4\to k_1,k_3,k_4.\end{aligned} \tag{3.7}$$

Thus

$$\sum_{\text{colors,spins}}|\mathfrak{M}_H|^2=-g^6F(k_1,-k_5,k_3,k_4,-k_2). \tag{3.8}$$

The overall minus arises from the antifermion spin sum

$$\sum_{\text{spins}}v(k)\bar{v}(k)=\not{k}=-(-\not{k}). \tag{3.9}$$

In Table I, we list the spin- and color-averaged squared matrix elements $\langle|\mathfrak{M}_j|^2\rangle$ in terms of the base functions F and G defined in (3.6).

We turn now to specifics of the functions F and G. The matrix elements $\mathfrak{M}$ for the process

$$q_A(p_1,i)+q_B(p_2,j)\to q_A(p_3,k)+q_B(p_4,l)+V(p_5,a) \tag{3.10}$$

can be written as a sum of five invariant amplitudes $\mathfrak{M}_j$, associated with the five diagrams in Fig. 7. Here, i,j,k,l,a are color indices. Writing

$$\mathfrak{M}_j=\mathfrak{M}_j^\mu\epsilon^{\mu*}, \tag{3.11}$$

where ϵ^μ is the polarization vector of V, and the terms $\mathfrak{M}_j^\mu$ are determined by the rules in Fig. 4 (in the Feynman gauge, $\alpha=1$):

TABLE I. Spin- and color-averaged squared matrix elements for single-gluon three-jet processes evaluated in terms of the functions F, G of Eqs. (3.14) and (3.20). The factors $[\frac{1}{2}]$ for processes (G) and (I) arise from final-state phase-space reduction for identical particles.

Process	$\langle\lvert\mathfrak{M}_j\rvert^2\rangle$
(F)	$(\frac{1}{36})F(p_1,p_2,p_3,p_4,p_5)$
(G)	$[\frac{1}{2}](\frac{1}{36})G(p_1,p_2,p_3,p_4,p_5)$
(H)	$-(\frac{1}{96})F(k_1,-k_5,k_3,k_4,-k_2)$
(I)	$-[\frac{1}{2}](\frac{1}{96})G(k_1,-k_5,k_3,k_4,-k_2)$
(J)	$(\frac{1}{36})F(k_1,-k_4,k_3,-k_2,k_5)$
(K)	$(\frac{1}{36})G(k_1,-k_4,k_3,-k_2,k_5)$
(L)	$(\frac{1}{36})F(k_1,-k_3,-k_2,k_4,k_5)$

$$
\begin{aligned}
(p_4-p_2)^2(p_3+p_5)^2\mathfrak{M}_1^\mu &= ig^3(T^bT^a)_{ik}T^b_{jl}[\bar{u}(p_3)\gamma^\mu(\not{p}_3+\not{p}_5)\gamma^\alpha u(p_1)][\bar{u}(p_4)\gamma^\alpha u(p_2)],\\
(p_4-p_2)^2(p_1-p_5)^2\mathfrak{M}_2^\mu &= ig^3(T^aT^b)_{ik}T^b_{jl}[\bar{u}(p_3)\gamma^\alpha(\not{p}_1-\not{p}_5)\gamma^\mu u(p_1)][\bar{u}(p_4)\gamma^\alpha u(p_2)],\\
(p_3-p_1)^2(p_4+p_5)^2\mathfrak{M}_3^\mu &= ig^3T^b_{ik}(T^bT^a)_{jl}[\bar{u}(p_3)\gamma^\alpha u(p_1)][\bar{u}(p_4)\gamma^\mu(\not{p}_4+\not{p}_5)\gamma^\alpha u(p_2)],\\
(p_3-p_1)^2(p_2-p_5)^2\mathfrak{M}_4^\mu &= ig^3T^b_{ik}(T^aT^b)_{jl}[\bar{u}(p_3)\gamma^\alpha u(p_1)][\bar{u}(p_4)\gamma^\alpha(\not{p}_2-\not{p}_5)\gamma^\mu u(p_2)],\\
(p_3-p_1)^2(p_4-p_2)^2\mathfrak{M}_5^\mu &= -g^3f_{abc}T^b_{ik}T^c_{jl}V^{\mu\eta\lambda}(p_5,p_3-p_1,p_4-p_2)[\bar{u}(p_3)\gamma^\eta u(p_1)][\bar{u}(p_4)\gamma^\lambda u(p_2)].
\end{aligned}
\tag{3.12}
$$

We shall, in fact, compute directly the traces for the squared matrix elements

$$
M_{ij}=M_{ji}\equiv\frac{1}{g^6}\sum_{\text{spins, colors}}\mathfrak{M}_i^{*\mu}\mathfrak{M}_j^\nu(\epsilon_\mu\epsilon_\nu^*)
\tag{3.13}
$$

from the six distinct cut closed-loop diagrams in Fig. 8. The objective function F is then given by

$$
F(p_1,p_2,p_3,p_4,p_5)=\sum_{i,j=1}^{5}M_{ij},
\tag{3.14}
$$

where we can identify

$$
\begin{aligned}
M_{11}&=T_{\mathrm{I}}(p_1,p_2,p_3,p_4,p_5),\\
M_{12}&=T_{\mathrm{IV}}(p_1,p_2,p_3,p_4,p_5),\\
M_{13}&=T_{\mathrm{III}}(p_1,p_2,p_3,p_4,p_5),\\
M_{14}&=T_{\mathrm{II}}(-p_3,-p_4,-p_1,-p_2,p_5),\\
M_{15}&=T_{\mathrm{V}}(-p_3,p_2,-p_1,p_4,p_5),\\
M_{22}&=T_{\mathrm{I}}(-p_3,p_2,-p_1,p_4,p_5),\\
M_{23}&=T_{\mathrm{II}}(p_1,p_2,p_3,p_4,p_5),\\
M_{24}&=T_{\mathrm{III}}(-p_3,-p_4,-p_1,-p_2,p_5),\\
M_{25}&=T_{\mathrm{V}}(p_1,p_2,p_3,p_4,p_5),\\
M_{33}&=T_{\mathrm{I}}(p_2,p_1,p_4,p_3,p_5),\\
M_{34}&=T_{\mathrm{IV}}(p_2,p_1,p_4,p_3,p_5),\\
M_{35}&=T_{\mathrm{V}}(-p_4,p_1,-p_2,p_3,p_5),\\
M_{44}&=T_{\mathrm{I}}(-p_4,p_1,-p_2,p_3,p_5),\\
M_{45}&=T_{\mathrm{V}}(p_2,p_1,p_4,p_3,p_5),\\
M_{55}&=T_{\mathrm{VI}}(p_1,p_2,p_3,p_4,p_5).
\end{aligned}
\tag{3.15}
$$

In (3.15), the functions T_J denotes the spin- and color-summed traces associated with diagrams in Fig. 8. The rules of Sec. III A give (removing the universal g^6 factor)

$$
\begin{aligned}
3(p_b\cdot p_d)^2(p_c\cdot p_e)T_{\mathrm{I}}&=2\,\mathrm{Tr}(\not{p}_e\gamma^\beta\not{p}_a\gamma^\alpha)\,\mathrm{Tr}(\not{p}_d\gamma^\beta\not{p}_b\gamma^\alpha),\\
48(p_a\cdot p_e)(p_a\cdot p_c)(p_d\cdot p_e)(p_b\cdot p_d)T_{\mathrm{II}}&=7\,\mathrm{Tr}[\gamma^\alpha\not{p}_a\gamma^\gamma\not{p}_c\gamma^\beta(\not{p}_a-\not{p}_e)]\,\mathrm{Tr}[\gamma^\alpha\not{p}_d\gamma^\beta\not{p}_b\gamma^\gamma(\not{p}_d+\not{p}_e)],\\
24(p_c\cdot p_e)(p_c\cdot p_a)(p_d\cdot p_e)(p_b\cdot p_d)T_{\mathrm{III}}&=\mathrm{Tr}[\gamma^\alpha\not{p}_c\gamma^\gamma\not{p}_a\gamma^\beta(\not{p}_c+\not{p}_e)]\,\mathrm{Tr}[\gamma^\alpha\not{p}_d\gamma^\beta\not{p}_b\gamma^\gamma(\not{p}_d+\not{p}_e)],\\
24(p_c\cdot p_e)(p_a\cdot p_e)(p_b\cdot p_d)^2T_{\mathrm{IV}}&=\mathrm{Tr}[\gamma^\alpha\not{p}_c\not{p}_a\gamma^\beta(\not{p}_c+\not{p}_e)(\not{p}_a-\not{p}_e)]\,\mathrm{Tr}(\not{p}_d\gamma^\beta\not{p}_b\gamma^\alpha),\\
16(p_a\cdot p_c)(p_a\cdot p_e)(p_b\cdot p_d)^2T_{\mathrm{V}}&=3V^{\alpha\beta\gamma}(p_e,p_c-p_a,p_d-p_b)\,\mathrm{Tr}[\not{p}_c\gamma^\beta\not{p}_a\gamma^\alpha(\not{p}_a-\not{p}_e)\gamma^\eta]\,\mathrm{Tr}(\not{p}_d\gamma^\gamma\not{p}_b\gamma^\eta),\\
8(p_a\cdot p_c)^2(p_b\cdot p_d)^2T_{\mathrm{VI}}&=-3V^{\alpha\beta\gamma}(p_e,p_c-p_a,p_d-p_b)V^{\alpha\delta\epsilon}(p_e,p_c-p_a,p_d-p_b)\,\mathrm{Tr}(\not{p}_c\gamma^\beta\not{p}_a\gamma^\delta)\,\mathrm{Tr}(\not{p}_d\gamma^\gamma\not{p}_b\gamma^\epsilon).
\end{aligned}
\tag{3.16}
$$

The functions $T_{\mathrm{I}}-T_{\mathrm{VI}}$ are given in terms of kinematic invariants in Appendix C.

Identical flavors. The formalism above must be expanded for identical quark flavors $A=B$ in Eq. (3.11). The matrix element $\mathfrak{M}$ is replaced by

$$
\mathfrak{N}=\mathfrak{M}-\tilde{\mathfrak{M}}=\left(\sum_{j=1}^{5}(\mathfrak{M}_j^\mu-\tilde{\mathfrak{M}}_j^\mu)\right)\epsilon^{\mu\,*},
\tag{3.17}
$$

where $\mathfrak{M}_j^\mu$ is obtained from $\mathfrak{M}_j^\mu$ by the interchange of the final fermion lines

$$(p_3, k) \leftrightarrow (p_4, l) . \tag{3.18}$$

Our objective function G,

$$G(p_1, p_2, p_3, p_4, p_5) \equiv \frac{1}{g^6} \sum_{\text{spins, colors}} |\mathfrak{M}|^2 , \tag{3.19}$$

can be written as

$$G(p_1, p_2, p_3, p_4, p_5) = F(p_1, p_2, p_3, p_4, p_5) + F(p_1, p_2, p_4, p_3, p_5) - 2\tilde{F}(p_1, p_2, p_3, p_4, p_5) , \tag{3.20}$$

where F is as defined above and

$$g^6 \tilde{F} \equiv \sum_{\text{color, spins}} \mathfrak{M}^* \tilde{\mathfrak{M}} . \tag{3.21}$$

We write $\tilde{F}$ as a sum

$$\tilde{F} = \sum_{i,j=1}^{5} \tilde{M}_{ij} , \tag{3.22}$$

where the 25 distinct terms

$$\tilde{M}_{ij} \equiv \frac{1}{g^6} \sum_{\text{colors, spins}} \mathfrak{M}_i^* \tilde{\mathfrak{M}}_j \tag{3.23}$$

can be evaluated in terms of the five cut diagrams shown in Fig. 9. Again removing the g^6 factor, the corresponding spin and color sums are given by

$$\begin{aligned}
&9(p_b \cdot p_c)(p_b \cdot p_d)(p_c \cdot p_e)(p_d \cdot p_e)\tilde{T}_{\mathrm{I}} = 80(p_a \cdot p_b)[p_d \cdot (p_c + p_e)][p_c \cdot (p_d + p_e)] , \\
&18(p_b \cdot p_c)(p_b \cdot p_d)(p_a \cdot p_e)(p_c \cdot p_e)\tilde{T}_{\mathrm{II}} = -\operatorname{Tr}[\not{p}_d \not{p}_c \not{p}_a \not{p}_b (\not{p}_a - \not{p}_e)(\not{p}_c + \not{p}_e)] , \\
&9(p_b \cdot p_c)(p_b \cdot p_d)(p_a \cdot p_e)\tilde{T}_{\mathrm{III}} = 64(p_d \cdot p_c)(p_b \cdot p_e) , \\
&8(p_a \cdot p_d)(p_b \cdot p_c)(p_b \cdot p_d)(p_c \cdot p_e)\tilde{T}_{\mathrm{IV}} = V^{\mu\lambda\eta}(p_e, p_c - p_b, p_d - p_a) \operatorname{Tr}[\not{p}_c \gamma^\lambda \not{p}_b \not{p}_a \gamma^\eta \not{p}_d (\not{p}_c + \not{p}_e)\gamma^\mu] , \\
&\tilde{T}_{\mathrm{V}} = 0 .
\end{aligned} \tag{3.24}$$

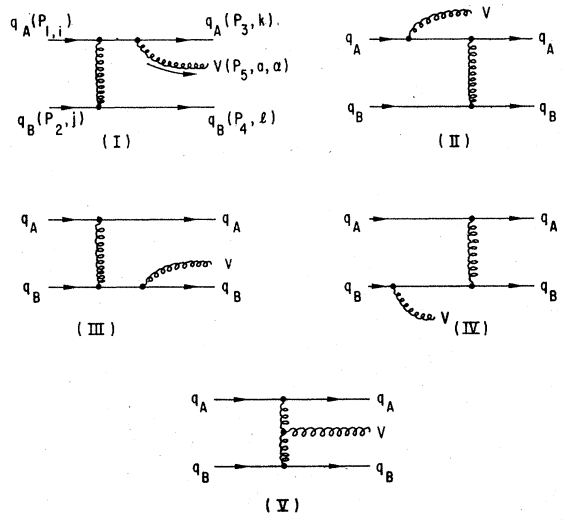

FIG. 7. The distinct Feynman diagrams for $q_A q_B \to q_A q_B V$. A, B represent distinct quark flavors.

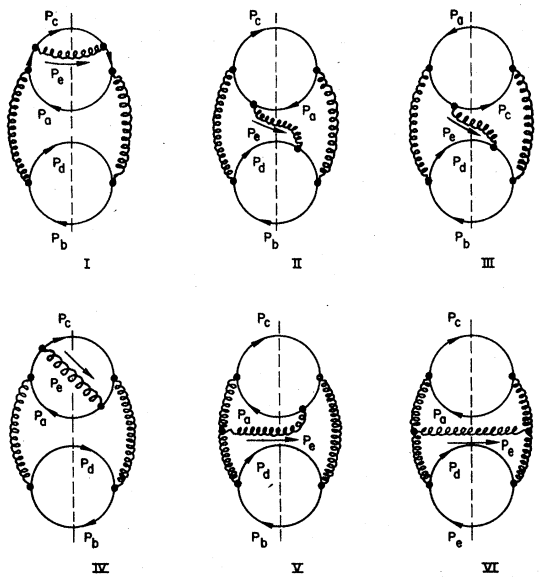

FIG. 8. Cut diagrams corresponding to the base functions T_{I}–T_{VI} in Eqs. (3.15) and (3.16).

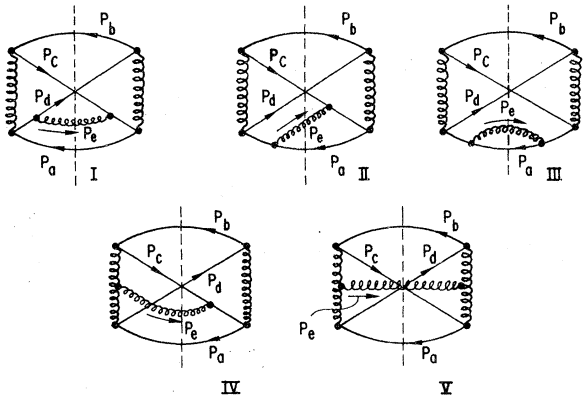

FIG. 9. Additional cut diagrams corresponding to the identical-particle interference traces in Eq. (3.24).

The color sum in $\tilde{T}_V$ vanishes. The required terms $\tilde{M}_{ij}$ needed in Eq. (3.22) are given by

$$
\begin{aligned}
\tilde{M}_{11} &= \tilde{T}_I(p_1,p_2,p_3,p_4,p_5)\,,\\
\tilde{M}_{12} &= \tilde{T}_{II}(p_1,p_2,p_3,p_4,p_5)\,,\\
\tilde{M}_{13} &= \tilde{T}_{III}(p_3,p_4,p_2,p_1,-p_5)\,,\\
\tilde{M}_{14} &= \tilde{T}_{II}(p_3,p_4,p_2,p_1,-p_5)\,,\\
\tilde{M}_{15} &= \tilde{T}_{IV}(p_1,p_2,p_3,p_4,p_5)\,,\\
\tilde{M}_{22} &= \tilde{T}_{III}(p_1,p_2,p_3,p_4,p_5)\,,\\
\tilde{M}_{23} &= \tilde{T}_{II}(p_3,p_4,p_1,p_2,-p_5)\,,\\
\tilde{M}_{24} &= \tilde{T}_{I}(p_4,p_3,p_1,p_2,-p_5)\,,\\
\tilde{M}_{25} &= \tilde{T}_{IV}(p_3,p_4,p_1,p_2,-p_5)\,,\\
\tilde{M}_{33} &= \tilde{T}_{I}(p_2,p_1,p_4,p_3,p_5)\,,\\
\tilde{M}_{34} &= \tilde{T}_{II}(p_2,p_1,p_4,p_3,p_5)\,,\\
\tilde{M}_{35} &= \tilde{T}_{IV}(p_2,p_1,p_4,p_3,p_5)\,,\\
\tilde{M}_{44} &= \tilde{T}_{III}(p_2,p_1,p_4,p_3,p_5)\,,\\
\tilde{M}_{45} &= \tilde{T}_{IV}(p_4,p_3,p_2,p_1,-p_5)\,,\\
\tilde{M}_{55} &= \tilde{T}_{V}(p_1,p_2,p_3,p_4,p_5)\,.
\end{aligned}
\tag{3.25}
$$

Terms not listed explicitly are obtained using

$$\tilde{H}_{ij}(p_1,p_2,p_3,p_4,p_5) = \tilde{H}_{ji}(p_1,p_2,p_4,p_3,p_5)\,. \tag{3.26}$$

The $\tilde{T}$'s of Eq. (3.25) can also be found in Appendix C.

Given the limited number of invariant amplitudes for $qq \to qqV$, explicit construction of the correspondence tables for M_{ij} terms is a relatively simple task. This approach is awkward for three-gluon processes (136 distinct M_{ij} terms) or five-gluon processes (325 terms). As an alternate method of evaluating the complete spin- and color-summed functions, one can work directly from the expressions for the cut diagrams. The total contribution from a given cut diagram is obtained by summing the value of the diagram over all distinct "permutations" of the cut lines. This will be our approach in subsequent sections, where the "permutations" will be more precisely defined.

C. Elementary $2 \to 3$ processes with three gluons

The basic transitions of interest here are

$$
\begin{aligned}
&\text{(P)}\quad q(l_1) + V(l_2) \to q(l_3) + V(l_4) + V(l_5)\,,\\
&\text{(Q)}\quad q(l_1) + \bar{q}(l_2) \to V(l_3) + V(l_4) + V(l_5)\,,\\
&\text{(R)}\quad V(l_1) + V(l_2) \to q(l_3) + \bar{q}(l_4) + V(l_5)\,.
\end{aligned}
\tag{3.27}
$$

A fourth process, $\bar{q}V \to \bar{q}VV$, is the charge on conjugate of (P) and is described by the same squared matrix element. In order to make the symmetries of these three-gluon processes most evident, we evaluate the spin- and color-summed functions in terms of that for a fourth, unphysical process

$$H(p_1,p_2,k_1,k_2,k_3) \equiv \frac{1}{g^6} \sum_{\text{color, spins}} \left|\mathfrak{M}(q(p_1) \to q(p_2) + V(k_1) + V(k_2) + V(k_3))\right|^2 . \tag{3.28}$$

The corresponding functions for P, Q, and R are obtained from H by simple crossings, as summarized in Table II.

The 16 invariant amplitudes contributing to $\mathfrak{M}$ are of four generic types as illustrated in Fig. 10. The complete sets of graphs is generated from this set by distinct relabelings of the external particles under the 12-fold permutation group generated by

(i) permutations of (k_1, k_2, k_3) and
(ii) Fermion line reversal $p_1 \longleftrightarrow -p_2$.

A word of caution is needed here. At the level of Feynman graphs, the permutation generator (ii) should be interpreted simply as reversal of the ordering of vertices along the Fermion line, without altering the spinors. The "analytic" interchange $p_1 \longleftrightarrow -p_2$ is an appropriate formulation of

TABLE II. Spin- and color-averaged squared matrix elements for triple-gluon three-jet processes evaluated in terms of the base function H in Eq. (3.29). Factors in square brackets represent identical-particle phase-space reduction.

Process	$\langle \lvert \mathfrak{M}_J \rvert^2 \rangle$
(P)	$[\frac{1}{2}](\frac{1}{96})H(l_1, l_3, -l_2, l_4, l_5)$
(Q)	$-[\frac{1}{6}](\frac{1}{36})H(l_1, -l_2, l_3, l_4, l_5)$
(R)	$-(\frac{1}{256})H(-l_4, l_3, -l_1, -l_2, l_5)$

this vertex reordering in the spin-summed cut diagrams discussed below.

Returning to Fig. 10, graph (I) has a twofold symmetry: $(p_1, p_2, k_1, k_3) \leftrightarrow (-p_2, -p_1, k_3, k_1)$. There are thus six distinct amplitudes of type I contributing to $\mathfrak{M}$. Graph (II) also contributes six amplitudes, with a twofold symmetry $k_2 \leftrightarrow k_3$. Graph (III) is fourfold symmetric under $k_2 \leftrightarrow k_3$, $p_1 \leftrightarrow -p_2$, giving three distinct terms. Graph (IV) is completely symmetric under the permutation group and contributes only once.

The 136 distinct terms $\mathfrak{M}_i^* \mathfrak{M}_j$ needed in evaluating H can be expressed in terms of 21 functions

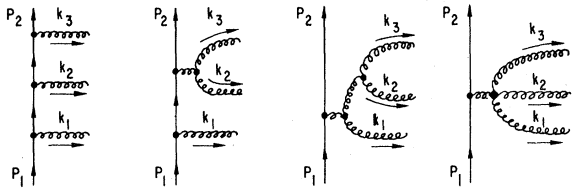

FIG. 10. Distinct classes of Feynman diagrams for $q \to qVVV$.

R_J corresponding to the cut diagrams shown in Fig. 11. We assign to each graph a weight W_J which is 1 for diagrams of the form $\mathfrak{M}_i^* \mathfrak{M}_i$ and 2 for interference terms $\mathfrak{M}_i^* \mathfrak{M}_j$, $i \neq j$. The spin- and color-summed function H is then given by

$$H = \sum_J W_J \Big(\sum_{\text{perms}}{}' R_J \Big), \tag{3.29}$$

where $\sum'_{\text{perms}} R_J$ indicates a sum over permutations which yield distinct values of R_J. Alternately,

$$H = \sum_J (W_J / N_J) \Big(\sum_{\text{perms}} R_J \Big), \tag{3.30}$$

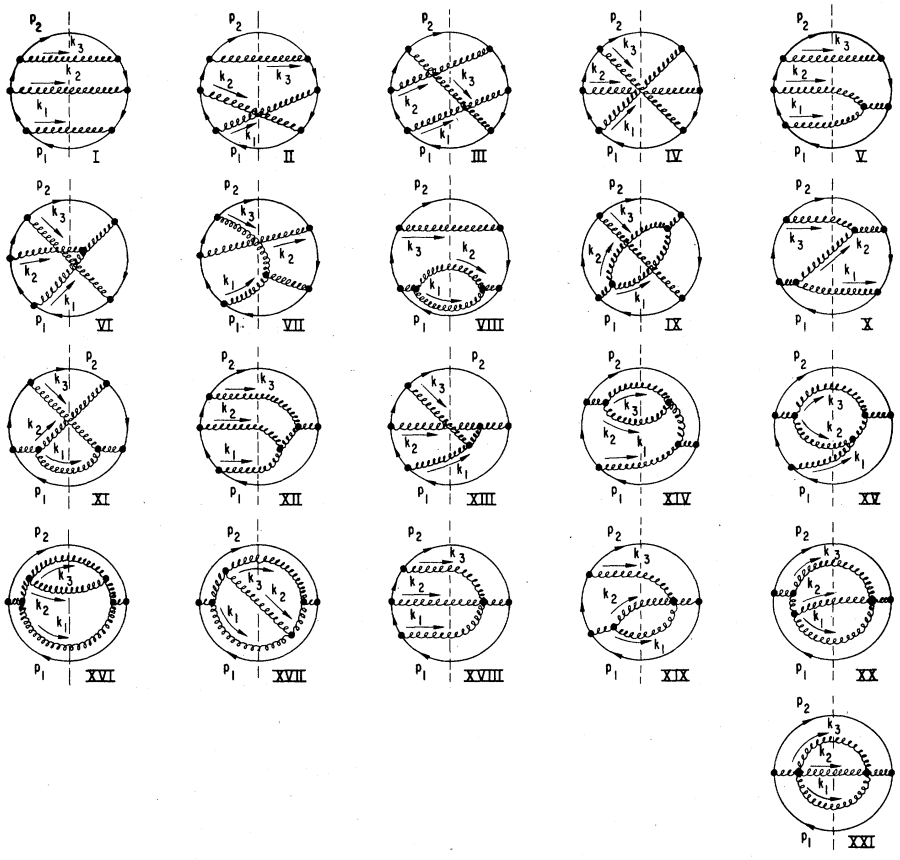

FIG. 11. Cut diagrams for $q \to qVVV$. The corresponding base functions are listed in Eq. (3.31).

where R_J is summed over all 12 permutations discussed above, and the symmetry factor N_J accounts for multiple counting. The symmetries, weights, and symmetry factors for the diagrams in Fig. 11 are listed in Table III.

Using the rules of Sec. III A, we obtain the following values for R_J (removing the universal g^6 factor):

$$
\begin{aligned}
&9(p_1\cdot k_1)(p_2\cdot k_3)R_{\mathrm{I}}=512(k_1\cdot k_3)\,,\\
&9(p_1\cdot k_1)(p_1\cdot k_2)(p_2\cdot k_3)R_{\mathrm{II}}=64(p_1\cdot k_3)(k_1\cdot k_2-p_1\cdot k_1-p_1\cdot k_2)\,,\\
&18(p_1\cdot k_1)(p_1\cdot k_3)(p_2\cdot k_3)(p_2\cdot k_2)R_{\mathrm{III}}=\mathrm{Tr}[\not p_2\not p_1(\not p_2+\not k_2)(\not p_2+\not k_3)(\not p_1-\not k_3)(\not p_1-\not k_1)]\,,\\
&9(p_1\cdot k_1)(p_1\cdot k_3)(p_2\cdot k_1)(p_2\cdot k_3)R_{\mathrm{IV}}=80(p_1\cdot p_2)(p_1\cdot p_2+p_1\cdot k_3-p_2\cdot k_3)(p_1\cdot p_2+p_1\cdot k_1-p_2\cdot k_1)\,,\\
&(p_1\cdot k_1)(p_2\cdot k_3)(k_1\cdot k_2)R_{\mathrm{V}}=-2V^{\alpha\beta\sigma}(k_1,k_2,-k_1-k_2)\,\mathrm{Tr}[\not k_3\gamma^\beta(\not p_1-\not k_1)\gamma^\alpha\not p_1\gamma^\sigma]\,,\\
&8(p_1\cdot k_1)(p_1\cdot k_3)(p_2\cdot k_3)(k_1\cdot k_3)R_{\mathrm{VI}}=-V^{\alpha\beta\sigma}(k_1,k_2,-k_1-k_2)\,\mathrm{Tr}[\not p_2\gamma^\sigma(\not p_1-\not k_3)(\not p_2+k_3)\gamma^\beta(\not p_1-\not k_1)\gamma^\alpha\not p_1]\,,\\
&8(p_1\cdot k_1)(p_2\cdot k_3)(p_2\cdot k_2)(k_1\cdot k_3)R_{\mathrm{VII}}=V^{\alpha\gamma\sigma}(k_1,k_3,-k_1-k_3)\,\mathrm{Tr}[\not p_2(\not p_1-\not k_1)\gamma^\alpha\not p_1\gamma^\sigma(\not p_2+\not k_2)(\not p_2+\not k_3)\gamma^\gamma]\,,\\
&(k_1\cdot k_2)^2(k_3\cdot p_2)R_{\mathrm{VIII}}=8L_1^{\rho\sigma}(k_1,k_2)\,\mathrm{Tr}[\not k_3\gamma^\sigma\not p_1\gamma^\rho]\,,\\
&2(p_1\cdot k_3)(p_2\cdot k_3)(k_1\cdot k_2)^2R_{\mathrm{IX}}=L_1^{\rho\sigma}(k_1,k_2)\,\mathrm{Tr}[\not p_2\not p_1\gamma^\sigma(\not p_2+\not k_3)(\not p_1-\not k_3)\gamma^\rho]\,,\\
&16(p_1\cdot k_1)(p_2\cdot k_3)(k_1\cdot k_2)(k_2\cdot k_3)R_{\mathrm{X}}\\
&\qquad=-9\,V^{\alpha\beta\sigma}(k_1,k_2,-k_1-k_2)V^{\gamma\beta\rho}(k_3,k_2,-k_2-k_3)\,\mathrm{Tr}[\not p_2\gamma^\gamma(\not p_2+\not k_3)\gamma^\sigma\not p_1\gamma^\alpha(\not p_1-\not k_1)\gamma^\rho]\,,\\
&R_{\mathrm{XI}}=0\,,\qquad\qquad(3.31)\\
&16(p_1\cdot p_2)(p_1\cdot k_1)(p_2\cdot k_3)(k_1\cdot k_2)R_{\mathrm{XII}}\\
&\qquad=-9V^{\alpha\beta\rho}(k_1,k_2,-k_1-k_2)V^{\gamma\rho\sigma}(-k_3,-k_1-k_2,k_1+k_2+k_3)\,\mathrm{Tr}[\not p_2\gamma^\gamma(\not p_2+\not k_3)\gamma^\beta(\not p_1-\not k_1)\gamma^\alpha\not p_1\gamma^\sigma]\,,\\
&R_{\mathrm{XIII}}=0\,,\\
&4(k_2\cdot k_3)^2(p_1\cdot p_2)(p_1\cdot k_1)R_{\mathrm{XIV}}=-9L_1^{\rho\sigma}(k_2,k_3)V^{\sigma\alpha\tau}(-k_2-k_3,-k_1,k_1+k_2+k_3)\,\mathrm{Tr}[\not p_2\gamma^\rho(\not p_1-\not k_1)\gamma^\alpha\not p_1\gamma^\tau]\,,\\
&16(p_1\cdot p_2)(p_1\cdot k_1)(k_2\cdot k_3)(k_2\cdot k_1)R_{\mathrm{XV}}=9L_2^{\alpha\rho\tau}(k_1,k_2,k_3)\,\mathrm{Tr}[\not p_2\gamma^\rho(\not p_1-\not k_1)\gamma^\alpha\not p_1\gamma^\tau]\,,\\
&4(p_1\cdot p_2)^2(k_2\cdot k_3)^2R_{\mathrm{XVI}}=-9L_3^{\sigma\tau}(k_1,k_2,k_3)\,\mathrm{Tr}[\not p_2\gamma^\sigma\not p_1\gamma^\tau]\,,\\
&8(p_1\cdot p_2)^2(k_2\cdot k_3)(k_2\cdot k_1)R_{\mathrm{XVII}}=-9L_4^{\sigma\tau}(k_1,k_2,k_3)\,\mathrm{Tr}(\not p_2\gamma^\sigma\not p_1\gamma^\tau)\,,\\
&8(p_1\cdot k_1)(p_2\cdot k_3)(p_1\cdot p_2)R_{\mathrm{XVIII}}=-9[K(\alpha\beta;\gamma\delta)+K(\alpha\delta;\gamma\beta)]\,\mathrm{Tr}[\not p_2\gamma^\gamma(\not p_2+\not k_3)\gamma^\beta(\not p_1-\not k_1)\gamma^\alpha\not p_1\gamma^\delta]\,,\\
&8(p_1\cdot p_2)(k_1\cdot k_2)(p_2\cdot k_3)R_{\mathrm{XIX}}=27K(\alpha\beta;\gamma\delta)V^{\alpha\beta\sigma}(k_1,k_2,-k_1-k_2)\,\mathrm{Tr}[\not p_2\gamma^\gamma(\not p_2+\not k_3)\gamma^\sigma\not p_1\gamma^\delta]\,,\\
&4(p_1\cdot p_2)^2(k_1\cdot k_2)R_{\mathrm{XX}}=-27K(\alpha\beta;\gamma\delta)\,\mathrm{Tr}(\not p_2\gamma^\tau\not p_1\gamma^\delta)V^{\tau\gamma\sigma}(k_1+k_2+k_3,-k_3,-k_1-k_2)V^{\alpha\beta\sigma}(k_1,k_2,-k_1-k_2)\,,\\
&(p_1\cdot p_2)R_{\mathrm{XXI}}=1944\,.
\end{aligned}
$$

The color sums for diagrams XI and XIII vanish. The tensors L_j in the above expressions arise from ghost corrections to closed gluon loops, as illustrated in Fig. 12, and are given by

$$
\begin{aligned}
&L_1^{\rho\sigma}(q_a,q_b)=4(q_a\cdot q_b)g^{\rho\sigma}-(q_a^\rho q_a^\sigma+q_b^\rho q_b^\sigma)-3(q_a^\rho q_b^\sigma+q_b^\rho q_a^\sigma)\,,\\
&L_2^{\alpha\rho\tau}(k_1,k_2,k_3)=V^{\beta\gamma\rho}(k_2,k_3,-k_2-k_3)V^{\alpha\beta\sigma}(k_1,k_2,-k_1-k_2)V^{\tau\sigma\gamma}(k_1+k_2+k_3,-k_1-k_2,-k_3)\\
&\qquad-(k_1^\alpha+k_2^\alpha)k_2^\rho k_3^\tau-k_2^\alpha k_3^\rho(k_1^\tau+k_2^\tau)\,,\\
&L_3^{\sigma\tau}(k_1,k_2,k_3)=V^{\beta\gamma\rho}(k_2,k_3,-k_2-k_3)V^{\beta\gamma\eta}(k_2,k_3,-k_2-k_3)V^{\alpha\rho\sigma}(-k_1,-k_2-k_3,k_1+k_2+k_3)\\
&\qquad\times V^{\alpha\eta\tau}(-k_1,-k_2-k_3,k_1+k_2+k_3)\\
&\qquad+(k_3^\rho k_2^\eta+k_2^\rho k_3^\eta)V^{\alpha\rho\sigma}(-k_1,-k_2-k_3,k_1+k_2+k_3)V^{\alpha\eta\tau}(-k_1,-k_2-k_3,k_1+k_2+k_3)\\
&\qquad+2(k_2\cdot k_3)[k_1^\sigma(k_2^\tau+k_3^\tau)+(k_2^\sigma+k_3^\sigma)k_1^\tau]\,,
\end{aligned}
\qquad(3.32)
$$

$$L_4^{\sigma\tau}(k_1,k_2,k_3) = V^{\alpha\eta\sigma}(-k_1,\,-k_2-k_3,\,k_1+k_2+k_3)V^{\alpha\beta\rho}(k_1,k_2,\,-k_1-k_2)V^{\beta\gamma\eta}(k_2,k_3,\,-k_2-k_3)$$
$$\times V^{\gamma\tau\rho}(-k_3,k_1+k_2+k_3,\,-k_1-k_2)$$
$$+V^{\gamma\tau\rho}(-k_3,k_1+k_2+k_3,\,-k_1-k_2)[k_2^\gamma(k_2^\sigma+k_3^\sigma)k_1^\rho+(k_2^\gamma+k_3^\gamma)k_1^\sigma k_2^\rho]$$
$$+V^{\alpha\sigma\eta}(-k_1,k_1+k_2+k_3,\,-k_2-k_3)[k_2^\eta k_3^\tau(k_1^\alpha+k_2^\alpha)+k_3^\eta(k_1^\tau+k_2^\tau)k_2^\alpha]$$
$$-(k_1\cdot k_3)(k_2^\sigma+k_3^\sigma)(k_1^\tau+k_2^\tau)-(k_1\cdot k_2+k_2\cdot k_3+k_1\cdot k_3)k_1^\sigma k_3^\tau\,.$$

Expressions for the R's of Eq. (3.31) are given in Appendix C.

D. The process $VV\to VVV$

The final elementary $2\to3$ process to be considered is

$$\text{(S)}\quad V(p_1)+V(p_2)\to V(p_3)+V(p_4)+V(p_5)\,.$$

We shall evaluate the five-gluon squared matrix element in the unphysical, symmetric configuration where all gluons are outgoing with momenta k_i. Denoting the corresponding spin- and color-summed function by $K(k_1,k_2,k_3,k_4,k_5)$, we obtain by crossing

$$\sum_{\text{colors, spins}}|\mathfrak{M}_S|^2 = g^6K(-p_1,\,-p_2,p_3,p_4,p_5)\,. \tag{3.33}$$

The 25 distinct amplitudes are of two types as shown in Fig. 13. Diagram I has three twofold symmetries, corresponding to the interchanges (i) $k_1 \leftrightarrow k_2$, (ii) $k_4 \leftrightarrow k_5$, and (iii) $(k_1,k_2)\leftrightarrow(k_4,k_5)$. There are thus $5!/(2^3)=15$ distinct amplitudes of this type. Diagram II has a twofold symmetry $k_1\leftrightarrow k_2$ and a sixfold symmetry for arbitrary permutations of (k_3,k_4,k_5), giving ten amplitudes.

The required 325 distinct product terms $\mathfrak{M}_i^*\mathfrak{M}_j$ can be evaluated in terms of the ten cut diagrams shown in Fig. 14. Denoting the spin- and color-summed functions for these diagrams by Q_J, the function K may be expanded as

$$K=\sum_{J=1}^{10}W_J\sum_{\text{perms}}{}'\,Q_J\,, \tag{3.34}$$

where $\sum'$ indicates a restriction of the sum to permutations of (k_1,k_2,k_3,k_4,k_5) which yield distinct values of Q_J. The weight factor W_J is 1 for $J=1$ and 8, and is 2 for the remaining interference terms. We again may reexpress the sum in Eq. (3.34) as a sum over all permutations of the momenta k_i by introducing multiple-counting symmetry factors N_J:

TABLE III. Symmetries, weights (W_J), and multiple-counting factors (N_J) for the basic triple-gluon cut diagrams in Fig. (11).

Term	W_J	Symmetries	N_J	No. of terms
I	1	$(p_1,p_2,k_1,k_3)\leftrightarrow(-p_2,-p_1,k_3,k_1)$	2	6
II	2	$k_1\leftrightarrow k_2$	2	6
III	2	$(p_1,p_2,k_1,k_2)\leftrightarrow(-p_2,-p_1,k_2,k_1)$	2	6
IV	2	$k_1\leftrightarrow k_3$; $(p_1,p_2)\leftrightarrow(-p_2,-p_1)$	4	3
V	2	none	1	12
VI	2	none	1	12
VII	2	none	1	12
VIII	1	$k_1\leftrightarrow k_2$	2	6
IX	2	$k_1\leftrightarrow k_2$; $(p_1,p_2)\leftrightarrow(-p_2,-p_1)$	4	3
X	2	$(p_1,p_2,k_1,k_3)\leftrightarrow(-p_2,-p_1,k_3,k_1)$	2	6
XI	2	$k_2\leftrightarrow k_3$	2	6
XII	2	none	1	12
XIII	2	$(p_1,p_2,k_1,k_3)\leftrightarrow(-p_2,-p_1,k_3,k_1)$	2	6
XIV	2	$k_2\leftrightarrow k_3$	2	6
XV	2	none	1	12
XVI	1	$k_2\leftrightarrow k_3$; $(p_1,p_2)\leftrightarrow(-p_2,-p_1)$	4	3
XVII	2	$k_1\leftrightarrow k_3$; $(p_1,p_2)\leftrightarrow(-p_2,-p_1)$	4	3
XVIII	2	$(p_1,p_2,k_1,k_3)\leftrightarrow(-p_2,-p_1,k_3,k_1)$	2	6
XIX	2	$k_1\leftrightarrow k_2$	2	6
XX	2	$k_1\leftrightarrow k_2$; $(p_1,p_2)\leftrightarrow(-p_2,-p_1)$	4	3
XXI	1	completely symmetric	12	1

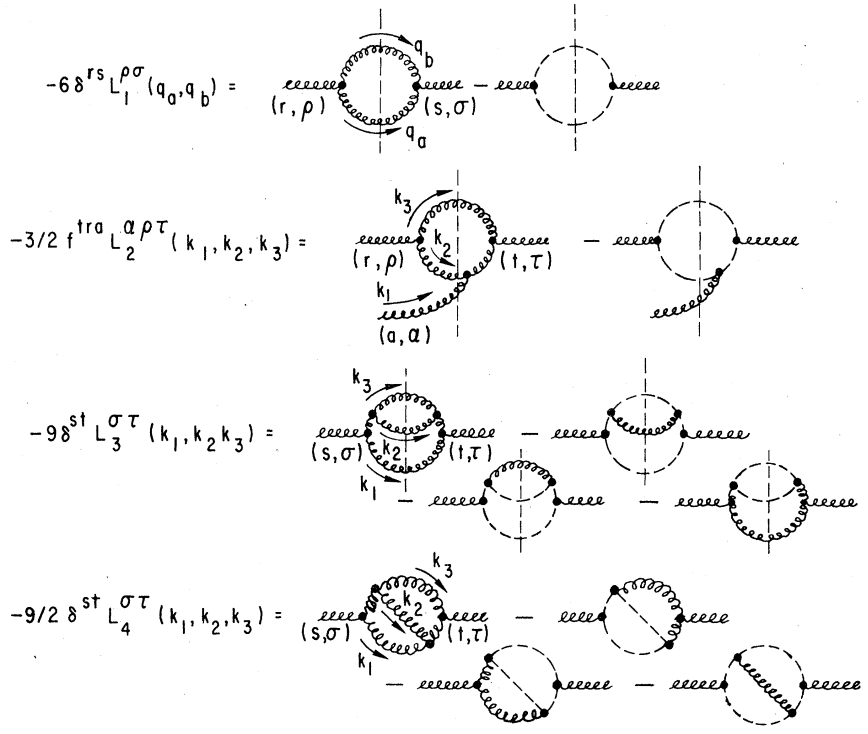

FIG. 12. Ghost-loop expansions for the tensors L_j in Eq. (3.32).

$$K=\sum_{J=1}^{10}(W_J/N_J)\sum_{\text{all perms}}Q_J\,. \tag{3.35}$$

The symmetries and weights corresponding to the ten cut diagrams in Fig. 14 are summarized in Table IV.

The color sum for $Q_{\rm III}$ vanishes. The expressions for $Q_{\rm I}$, $Q_{\rm II}$, and $Q_{\rm IV}$ are a bit lengthy due to the large number of ghost contributions and are given in Appendix B. Diagrams V–VIII each require a single ghost loop corresponding to the outer gluon circle. Diagrams IX and X admit no ghosts. The corresponding Q_J terms are given here:

$$\begin{aligned}
&4(k_1\cdot k_2)(k_1\cdot k_5)(k_4\cdot k_5)Q_{\rm V}\\
&\qquad=27[K(\beta\gamma;\,\delta\sigma)+K(\beta\sigma;\,\delta\gamma)]\\
&\qquad\quad\times[V^{\alpha\beta\rho}(k_1,k_2,\,-k_1-k_2)V^{\rho\gamma\eta}(k_1+k_2,k_3,k_4+k_5)V^{\delta\epsilon\,\eta}(k_4,k_5,\,-k_4-k_5)V^{\alpha\epsilon\sigma}(k_1,k_5,\,-k_1-k_5)\\
&\qquad\quad+(k_1^\beta+k_2^\beta)(k_4^\gamma+k_5^\gamma)k_5^\delta k_1^\sigma+k_1^\beta(k_1^\gamma+k_2^\gamma)(k_4^\delta+k_5^\delta)k_5^\sigma]\,,\\
&4(k_1\cdot k_2)(k_3\cdot k_4)(k_1\cdot k_5)Q_{\rm VI}=-81K(\beta\sigma;\,\gamma\delta)V^{\gamma\delta\eta}(k_3,k_4,\,-k_3-k_4)\\
&\qquad\quad\times[V^{\alpha\beta\rho}(k_1,k_2,\,-k_1-k_2)V^{\rho\eta\epsilon}(k_1+k_2,k_3+k_4,k_5)V^{\alpha\epsilon\sigma}(k_1,k_5,\,-k_1-k_5)\\
&\qquad\quad+k_1^\beta(k_1^\eta+k_2^\eta)k_5^\sigma+(k_1^\beta+k_2^\beta)k_5^\eta k_1^\sigma]\,,\\
&2(k_1\cdot k_5)^2(k_3\cdot k_4)Q_{\rm VII}=-81K(\beta\tau;\,\delta\gamma)V^{\gamma\delta\eta}(k_3,k_4,\,-k_3-k_4)V^{\beta\eta\rho}(k_2,k_3+k_4,k_1+k_5)\\
&\qquad\quad\times[V^{\alpha\epsilon\rho}(k_1,k_5,\,-k_1-k_5)V^{\alpha\epsilon\tau}(k_1,k_5-k_1-k_5)+k_1^\rho k_5^\tau+k_5^\rho k_1^\tau]\,,\\
&(k_1\cdot k_5)Q_{\rm VIII}=-29160\,,\\
&(k_1\cdot k_4)(k_1\cdot k_5)Q_{\rm IX}=-27[2K(\beta\gamma;\,\delta\sigma)K(\beta\gamma;\,\epsilon\rho)+K(\beta\delta;\,\gamma\sigma)K(\beta\rho;\,\epsilon\gamma)]\\
&\qquad\quad\times V^{\alpha\epsilon\sigma}(k_1,k_5,\,-k_1-k_5)V^{\alpha\delta\rho}(k_1,k_4,\,-k_1-k_4)\,,\\
&2(k_1\cdot k_5)(k_2\cdot k_4)Q_{\rm X}=243K(\alpha\epsilon;\,\gamma\tau)K(\beta\delta;\,\gamma\sigma)V^{\alpha\epsilon\sigma}(k_1,k_5,-k_1-k_5)V^{\beta\delta\tau}(k_2,k_4,\,-k_2-k_4)\,.
\end{aligned} \tag{3.36}$$

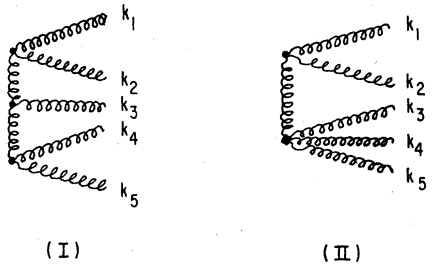

FIG. 13. Distinct classes of Feynman diagrams for the five-gluon process.

Complete expressions in terms of invariants for the Q's can be found in Appendix C.

IV. RESULTS

We would now like to use the cross sections calculated in Sec. III to make some simple numerical estimates of three-jet production. One of the most straightforward things we can do is to compare at fixed E_T the relative importance of three-jet configurations and two-jet configurations. This will serve to illustrate our formalism. More complicated calculations will not be considered at this time.

Idealized transverse cross sections. We use the kinematic variables for three-jet production in (2.40)–(2.42) in the limit when all jets are produced at 90° in the c. m. system and neglecting effects proportional to δ, ϵ. After spin and color averaging, the squared matrix elements for the $2 \to 3$ processes in this configuration can be written

$$\langle |\mathfrak{M}_{ab\to 123}|^2 \rangle \to \frac{(4\pi\alpha_s)^3}{x_T{}^2 S} A_{ab\to 123}(\hat{x}_1, \hat{x}_2) . \tag{4.1}$$

We can define the three-jet cross section

$$\Sigma^{(3)} \equiv \left. \frac{d\sigma^3}{dw\, d(\cos\theta_n)} \right|_{w=0,\ \cos\theta_n=\pm 1} , \tag{4.2}$$

where $w = x_a - x_b$. Inserting (2.42), (4.1), and (4.2) into (2.31), we can write the cross section

$$\frac{d\Sigma^{(3)}_{AB}}{dx_T d\hat{x}_1 d\hat{x}_2} \cong \left(\frac{\alpha_s{}^3}{4x_T{}^2 S}\right) \sum_{ab\to 123} \tilde{G}^{\delta}_{a/A}(x_T) \tilde{G}^{\delta}_{b/B}(x_T) \times A_{ab\to 123}(\hat{x}_1, \hat{x}_2) . \tag{4.3}$$

We would like an analogous expression for the transverse two-jet cross section. We define

$$\Sigma^{(2)}_{AB} \equiv \left. \frac{2 d\sigma^{2\ \text{jet}}_{AB}}{dw\, d(\cos\theta_1)} \right|_{\substack{w=0 \\ \cos\theta_1=0}} , \tag{4.4}$$

and the color- and spin-averaged squared matrix element

$$\langle |\mathfrak{M}_{ab\to 12}|^2 \rangle = 16\pi^2 \alpha_s{}^2 B_{ab\to 12} . \tag{4.5}$$

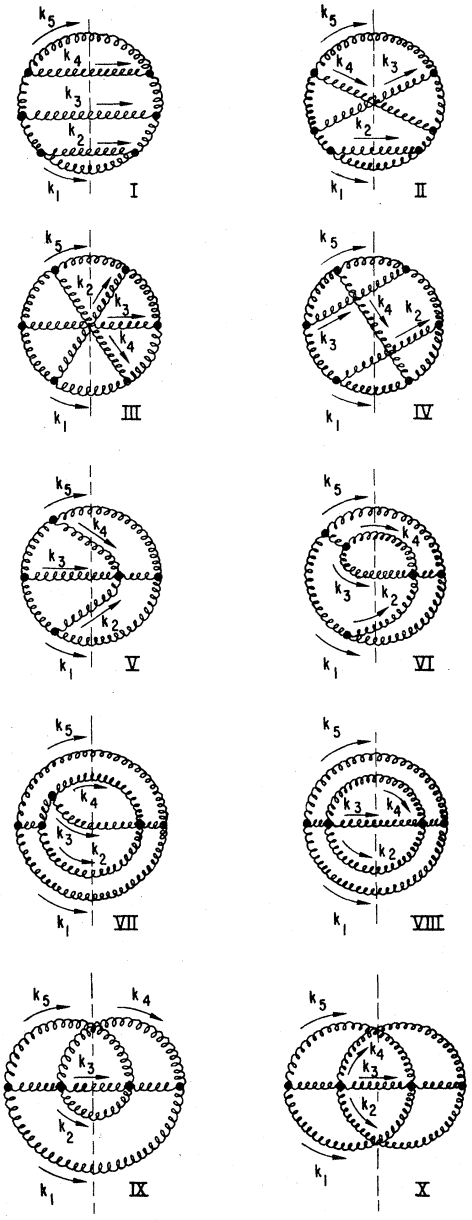

FIG. 14. The ten distinct cut diagrams used to evaluate $|\mathfrak{M}|^2$ for $VV \to VVV$.

Inserting these into the hard-scattering model Eq. (2.1) gives

$$\frac{d\Sigma^{(2)}}{dx_T d\hat{x}_1 d\hat{x}_2} \cong \frac{\pi\alpha_s{}^2}{x_T{}^2 S} \sum_{ab\to 12} \tilde{G}^{\delta}_{a/A}(x_T) \tilde{G}^{\delta}_{b/B}(x_T) B_{ab\to 12} \times \delta(1-\hat{x}_1)\delta(1-\hat{x}_2) . \tag{4.6}$$

The functions $A_{ab\to 123}(\hat{x}_1, \hat{x}_2)$ are obtained from the squared matrix elements in Sec. III by the dot-product substitutions of Eq. (2.41). All the functions increase toward the edges of the Dalitz plot

TABLE IV. Symmetries, weights, and multiple-counting factors for the basic five-gluon cut diagrams in Fig. 14.

Term	W_J	Symmetries	N_J	No. of terms
I	1	$k_1 \longleftrightarrow k_2; k_4 \longleftrightarrow k_5$ $(k_1,k_2) \longleftrightarrow (k_4,k_5)$	8	15
II	2	$k_1 \longleftrightarrow k_2; k_3 \longleftrightarrow k_4$	4	30
III	2	$k_1 \longleftrightarrow k_5; k_2 \longleftrightarrow k_4$ $(k_1,k_2,k_4,k_5) \longleftrightarrow (k_2,k_1,k_5,k_4)$	8	15
IV	2	$(k_1,k_2) \longleftrightarrow (k_5,k_3)$	2	60
V	2	$(k_1,k_2) \longleftrightarrow (k_5,k_4)$	2	60
VI	2	$k_3 \longleftrightarrow k_4$	2	60
VII	2	$k_1 \longleftrightarrow k_5; k_4 \longleftrightarrow k_3$	4	30
VIII	1	$k_1 \longleftrightarrow k_5$ all perms. of (k_2,k_3,k_4)	12	10
IX	2	$k_4 \longleftrightarrow k_5; k_2 \longleftrightarrow k_3$	4	30
X	2	$k_1 \longleftrightarrow k_5; k_2 \longleftrightarrow k_4$ $(k_1,k_5) \longleftrightarrow (k_2,k_4)$	8	15

so we can obtain a crude lower estimate of identifiable three-jet events by looking at the symmetric value

$$A^{\rm sym}_{ab\to 123} \equiv A_{ab\to 123}(\hat{x}_1=\hat{x}_2=\hat{x}_3=\tfrac{2}{3}) \ . \tag{4.7}$$

Values of $A^{\rm sym}$ for the various three-jet processes are listed in Table V. Factors in angular brackets arise from summing over quark flavors in pair production processes and from identical-particle phase-space reduction. For comparison, we list in Table VI the constants B defined in (4.5) for the $2\to 2$ processes.

It is convenient to introduce notation for the weighted sums of distribution functions occuring in the cross section formulas (4.3) and (4.6). We define

$$\begin{aligned} C^2_{AB}(x_T) &\equiv \sum_{ab\to 12} \tilde{G}^{\delta}_{a/A}(x_T)\tilde{G}^{\delta}_{b/B}(x_T)B_{ab\to 12} \ , \\ C^3_{AB}(x_T) &\equiv \sum_{ab\to 123} \tilde{G}^{\delta}_{a/A}(x_T)\tilde{G}^{\delta}_{b/B}(x_T)A^{\rm sym}_{ab\to 123} \ . \end{aligned} \tag{4.8}$$

The transverse cross sections $\Sigma(x_T) \equiv d\Sigma/dx_T$ are given by

$$\Sigma^{2\ \rm jet}(x_T) = \left(\frac{\pi\alpha_s^{\,2}}{x_T^{\,2}s}\right) C^2_{AB}(x_T) \ , \tag{4.9}$$

$$\begin{aligned} \Sigma^{3\ \rm jet}_{\rm sym}(x_T) &\equiv \frac{d\Sigma^{3\ \rm jet}}{dx_T\, d\hat{x}_1 d\hat{x}_2}\bigg|_{\hat{x}_1=\hat{x}_2=2/3} \\ &= \frac{\alpha_s^{\,3}}{4x_T^{\,2}s} C^3_{AB}(x_T) \ , \end{aligned} \tag{4.10}$$

TABLE V. Spin- and color-averaged squared matrix elements for three-jet processes evaluated in the symmetric configuration, as defined in Eq. (4.7).

Process	$A_{\rm sym}$	
$q_A q_B \to q_A q_B V$	320/3	106.7
$q_A q_A \to q_A q_A V$	$\langle\frac{1}{2}\rangle$(160)	80.0
$q_A V \to q_A q_B \bar{q}_B$	$\langle 2\rangle$(64/9)	14.2
$q_A V \to q_A q_A \bar{q}_A$	$\langle\frac{1}{2}\rangle$(416/27)	7.7
$q_A \bar{q}_B \to q_A \bar{q}_B V$	160	160.0
$q_A \bar{q}_A \to q_A \bar{q}_A V$	1552/9	172.4
$q_A \bar{q}_A \to q_B \bar{q}_B V$	$\langle 2\rangle$(224/27)	16.6
$q_A V \to q_A VV$	$\langle\frac{1}{2}\rangle$17 918/27	331.8
$VV \to q_B \bar{q}_B V$	$\langle 3\rangle$(119/4)	89.3
$q_A \bar{q}_A \to VVV$	$\langle\frac{1}{6}\rangle$368/3	20.44
$VV \to VVV$	$\langle\frac{1}{6}\rangle$7290	1215

TABLE VI. Spin- and color-averaged squared matrix elements for two-jet processes at 90° in the parton c.m.

Process	B	
$q_A q_B \to q_A q_B$	20/9	2.22
$q_A q_A \to q_A q_A$	$\langle\frac{1}{2}\rangle$(88/27)	1.63
$q_A \bar{q}_B \to q_A \bar{q}_B$	20/9	2.22
$q_A \bar{q}_A \to q_A \bar{q}_A$	$\langle 2\rangle$(2/9)	0.44
$q_A \bar{q}_A \to q_A \bar{q}_A$	70/27	2.59
$q_A \bar{q}_A \to VV$	$\langle\frac{1}{2}\rangle$28/27	0.52
$q_A V \to q_A V$	55/9	6.11
$VV \to q_B \bar{q}_B$	$\langle 3\rangle$(7/48)	0.44
$VV \to VV$	$\langle\frac{1}{2}\rangle$243/8	15.19

so that

$$\frac{\Sigma^{3\ \text{jet}}_{\text{sym}}(x_T)}{\Sigma^{2\ \text{jet}}(x_T)} = \left(\frac{\alpha_s}{4\pi}\right)\frac{C^3_{AB}(x_T)}{C^2_{AB}(x_T)} . \tag{4.11}$$

For comparison, we note that the corresponding expression in e^+e^- annihilation is

$$\frac{\sigma^{\text{sym}}(e^+e^-\to q\bar{q}V)}{\sigma(e^+e^-\to q\bar{q})} = \left(\frac{\alpha_s}{4\pi}\right)\left(\frac{64}{3}\right) . \tag{4.12}$$

There are corrections of $O(\alpha)$ to (4.11) and (4.12) from virtual corrections to the two-jet cross section. For most cases, these have not yet been calculated.

In Fig. 15 we plot the ratio C^3/C^2 vs x_T. Since the effects of scaling violations and of the δ veto should approximately cancel in this ratio, we have used Field-Feynman[8] quark distributions and a simple counting rule ansatz for the gluon distribution. Also shown is the constant value for e^+e^- annihilation. The fact that this ratio is 3–4 times bigger in large-p_T hadron collisions than in e^+e^- annihilation is important. Identifiable three-jet events should be correspondingly more common in hadron-hadron collisions.

The x_T dependence of the ratio $C^3(x_T)/C^2(x_T)$ can be understood in terms of the makeup of the different processes. As $x_T\to 0$, the VV initial state dominates both C^3 and C^2, and

$$\lim_{x_T\to 0} C^3(x_T)/C^2(x_T) \cong 80 . \tag{4.13}$$

At large x_T, the ratio is dominated by valence quarks,

$$\lim_{x_T\to 0} C^3(x_T)/C^2(x_T) \cong \begin{cases} 50 & (pp) \\ 60 & (\bar{p}p) \end{cases} . \tag{4.14}$$

The makeup of the symmetric three-jet states as a function of x_T are shown in Fig. 16 for our simple models for the distribution functions. In this figure we do not distinguish q from $\bar{q}$. The $qq\bar{q}$ final state never contributes more than 2% and is not included. Multigluon states are dominant for $x_T \lesssim 0.6$ indicating that detailed analyses of three-jet production using only the process $qq\to qqV$[19,20] should only be applied at very large x_T.

We can now use these numbers to estimate the number of three-jet events. For simplicity we will define candidate three-jet events in terms of a thrust cut. We can get a lower bound on the number of three-jet events by integrating (4.3) subject to $\max(x_i) < (T_C+1)/2$, with the approximation that $A(x_1,x_2) = A^{\text{sym}}$ within the allowed region. This gives an approximation of the ratio of three-jet to two-jet events,

$$R(x_T, T_C) \lesssim \frac{\alpha_s}{\pi}\left(\frac{C^3(x_T)}{C^2(x_T)}\right)\frac{3(T_C-1)^2}{32} . \tag{4.15}$$

We need to choose T_C small enough so that most of the two-jet events survive the smearing of the δ functions in (4.6) implied by nonperturbative effects. A conservative choice of $T_C = 0.75$ and $\alpha_s \cong 0.15$ gives

$$R(x_T, T_C) \lesssim 2.4\times 10^{-3}[C^3(x_T)/C^2(x_T)] \approx 0.2, \quad x_T \sim 0.2$$
$$\approx 0.1, \quad x_T \sim 0.8 . \tag{4.16}$$

These crude estimates suggest that transverse thrust distributions in large-p_T production of hadrons should be fairly broad compared to the thrust distributions observed in e^+e^- annihilations.

A more complete analysis of the event shape implied by the three-jet production processes of QCD will not be attempted here. Our preliminary efforts indicate that the situation in large-p_T hadron-hadron collisions is sufficiently different from e^+e^- annihilations to warrant detailed study. We have shown that it is possible to use experimental configurations incorporating vetos to control uncertainties associated with the initial partons to define interesting high-p_T jet cross sections and that these cross sections reflect the structure of perturbative QCD.

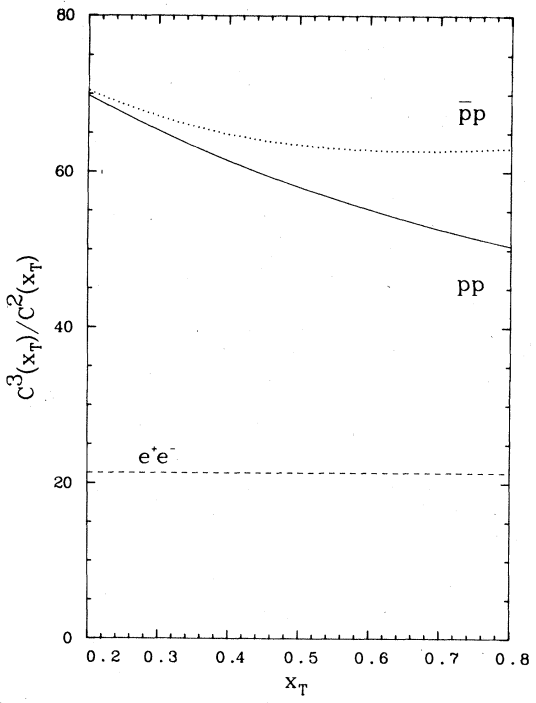

FIG. 15. The ratio $C^3_{AB}(x_T)/C^2_{AB}(x_T)$ as used in Eq. (4.11). The curves are calculated using Field-Feynman scaling-rule quark distributions and a counting-rule gluon distribution $xV(x) = 3(1-x)^5$. The corresponding constant value for e^+e^- annihilation is shown as a dashed line.

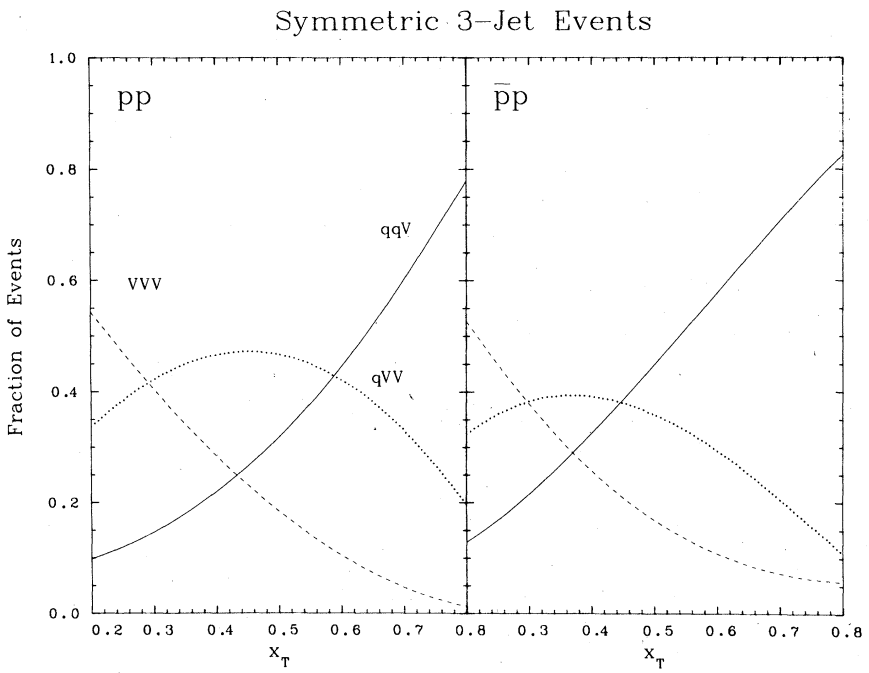

FIG. 16. Fractions of symmetric three-jet cross section for different final states versus x_T. The curves are for Field-Feynman quark distributions and a counting-rule gluon distribution.

ACKNOWLEDGMENTS

We are grateful to R. Field and E. Monsay for advice and conversations during the course of this work. Traces and dot products in the text have been evaluated using the algebraic manipulation program ASHMEDAI. This work was performed under the auspices of the United States Department of Energy.

APPENDIX A: THE DISTRIBUTIONS $G^{\delta}_{a/p}(x,k_T,\xi)$

In order to keep track of the hard central processes in pp collisions without ambiguity or double counting, it was seen to be convenient to introduce the veto-restricted distribution functions $G^{\delta}_{a/p}(x, k_T, \xi)$, where $\xi = \ln(P^2/\Lambda^2)$, with $P^2 = s/4$ and $\Lambda \cong 0.3$–0.7 GeV. The experimental situation envisioned includes a veto on any particle or group of particles with fractional energy $x \gtrsim \epsilon$ emerging with an angle $\gtrsim\delta$ from the direction of the initial hadron in the c. m. system. These distributions are clearly not identical with those familiar in completely inclusive processes although they reduce to the usual ones in the limit $\delta \to \pi/2$. The functions also depend on ϵ, but we will not show the ϵ dependence explicitly in what follows. It is primarily important for x near 0 or 1.

To lowest order in the perturbation theory, there are two contributions to the probability that an otherwise acceptable hard-scattering event will be vetoed. These are indicated schematically in Fig. 17. In many specific models for the bound-state wave function, contributions of the type illustrated in Fig. 17(b) were one of the "spectator" constituents in the hadron fragments to produce jets in the veto counter are suppressed. The precise nature of the suppression depends on the number of constituents in the hadron and on the possible "correlations" in the wave function, but, for our purposes, we will assume that we can get an adequate representation of the properties of the veto-restricted distributions by considering only diagrams of the type in Fig. 17(a).

For the k_T-integrated distribution functions we can write to lowest order

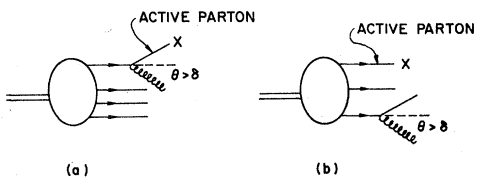

FIG. 17. Lowest-order processes leading to a δ veto of a hard-scattering event.

$$G^{\delta}_{a/p}(x,\ \ln P^2) \cong G_{a/p}(x,\ \ln P^2)\left[1 - \frac{\alpha}{2\pi}\ln\left(\frac{k_{T\,\max}{}^2}{k_T{}^2(\delta)}\right)\sum_b \int_{x+\epsilon}^1 \frac{dy}{y} G_{b/p}(y,\ \ln P^2) P_{a/b}(x/y)\right], \tag{A1}$$

where $G_{a/p}(x,\ \ln P^2)$ is the usual (nonscaling) parton distribution function, $P_{a/b}(x)$ are the Altarelli-Parisi probabilities[32] for partons, and the logarithm is

$$\ln\left(\frac{k_{T\,\max}{}^2}{k_T{}^2(\delta)}\right) \simeq \ln\left(\frac{(1-x)^2P^2}{(1-x)^2P^2\sin^2\delta}\right) = |\ln(\sin^2\delta)|. \tag{A2}$$

Neglecting terms of order ϵ, $\sin\delta$, we can see it is possible to incorporate (A1) into the Altarelli and Parisi master equations[32] at the price of making the effective scaling variable

$$\xi_\delta = \ln\left(\frac{P^2\sin^2\delta}{\Lambda^2}\right). \tag{A3}$$

The equations can be written

$$\frac{d}{d\xi_\delta}G^{\delta}_{q_i/p}(x,\ \xi_\delta) \cong \frac{\alpha(\xi_\delta)}{2\pi}\int_x^1 [G^{\delta}_{q_i/p}(x,\ \xi_\delta)P_{q/q}(x/y) + G_{V/p}(x,\ \xi_\delta)P_{q/V}(x,\ y)]\frac{dy}{y},$$

$$\frac{d}{d\xi_\delta}G^{\delta}_{V/p}(x,\ \xi_\delta) \cong \frac{\alpha(\xi_\delta)}{2\pi}\int_x^1 \left(\sum_f G^{\delta}_{q_f/p}(x,\ \xi_\delta)P_{V/q}(x/y) + G^{\delta}_{V/p}(x,\ \xi_\delta)P_{V/V}(x/y)\right)\frac{dy}{y}. \tag{A4}$$

These equations indicate that the scaling violations of the distributions $G^{\delta}_{a/p}(x, \xi_\delta)$ in the variable ξ_δ should be similar to the scaling violations of the usual inclusive distribution functions in the variable

$$\xi = \ln\left(\frac{P^2}{\Lambda^2}\right).$$

These scaling violations can, in principle, be studied by doing large-p_T hadron production at fixed p_T with a 4π detector and varying the angle δ in the veto in the off-line analysis of events.

Let us now turn to the k_T dependence of the veto-restricted distribution functions. We follow the formalism of Lam and Yan[33,34] to write the equation for the scaling violations

$$\frac{d}{d\xi_\delta}G^{\delta}_{a/p}(x,\vec{k}_T,\ \xi_\delta) \cong \frac{\alpha(\xi_\delta)}{2\pi}\sum_b \int dy\,dz\,d^2\vec{k}_{T1}d^2\vec{k}_{T2}\delta(x-yz) \times \delta^{(2)}(\vec{k}_T - z\vec{k}_{T1} - \vec{k}z_{T2})P^{\delta}_{a/b}(z,\ k_{T2})G^{\delta}_{b/p}(y,\ k_{T1},\ \xi_\delta). \tag{A5}$$

The condition that the jet p_2 not be directed into the veto counter can be approximated

$$k_{T2}{}^2 \lesssim (z^2P^2\sin^2\delta),$$

so that we can write

$$P^{\delta}_{a/b}(z,\ k_{T2}) \cong \frac{1}{\pi}P_{a/b}(z)\delta(k_{T2}{}^2 - z^2\exp(\xi_\delta)). \tag{A6}$$

It is instructive at this point to transform (A5) into impact-parameter space

$$G^{\delta}_{a/p}(x,\ b,\ \xi_\delta) = \frac{1}{(2\pi)}\int d^2\vec{k}_T e^{i\vec{b}\cdot\vec{k}_T}G^{\delta}_{a/p}(x,\ k_T,\ \xi_\delta) = \tfrac{1}{2}\int_0^\infty J_0(bk_T)G^{\delta}_{a/p}(x,\ k_T,\ \xi_\delta)d(k_T{}^2). \tag{A7}$$

We can then write (A5) in the form

$$\frac{d}{d\xi_\delta}G^{\delta}_{a/p}(x,b,\xi_\delta) \cong \frac{\alpha(\xi_\delta)}{2\pi}\sum_b\int_x^1\frac{dz}{z}P_{a/b}(z)J_0((bzP\sin\delta)/\Lambda) \times G^{\delta}_{b/p}(x/z,\ zb,\ \xi\delta). \tag{A8}$$

The oscillations of the Bessel function for $b \gg (zP\sin\delta)^{-1}$ give the approximate cutoff

$$k_T{}^2 \lesssim (1-x)^2P^2\sin^2\delta, \tag{A9}$$

given in Sec. II. Notice that the impact-parameter equation does not, in general, decouple to become an algebraic equation if we take moments in x. If, however, we assume

$$G^{\delta}_{a/p}(x,\ b,\ \xi_\delta) \cong H^{\delta}_{a/p}(x)F(xb),$$

where $F(xb)$ is independent of type, then we can pull $F(xb)$ out of the integral in (A8).

We shall not go further into the characteristics of the veto-restricted distribution functions. From (A1), (A4), (A8), and (A9), we can see that they are reasonable extensions of the usual inclusive distribution functions with properties which can be approximately taken into account in the calculation of quasiexclusive jet cross sections. Assuming the general arguments concerning the factorization of multijet cross sections in QCD

are correct,[3-5] these distribution functions can be measured in deep-inelastic lepton scattering experiments with a similar veto requirement built into the hadron fragmentation region.

APPENDIX B: FIVE-GLUON GHOST LOOPS

We list here the complete ghost-loop expansions corresponding to the diagrams I, II, and IV in Fig. 14.

1. $Q_{\rm I}$

Removing the overall factor of g^6, we can write

$$2(k_1\cdot k_2)^2(k_4\cdot k_5)^2 Q_{\rm I} = L_0^1 - \sum_{j=1}^{10} L_j^1 + \sum_{k=11}^{15} L_k^1 . \quad \text{(B1)}$$

L_0^1 corresponds to the ghostless diagram in Fig. 14,

$$L_0^1 = -27 V^{\alpha\beta\rho}(k_1, k_2, -k_1-k_2) V^{\alpha\beta\sigma}(k_1, k_2, -k_1-k_2) V^{\epsilon\delta\eta}(k_5, k_4, -k_5-k_4) V^{\epsilon\delta\tau}(k_5, k_4, -k_5-k_4)$$
$$\times V^{\gamma\eta\rho}(k_3, k_4+k_5, k_1+k_2) V^{\gamma\tau\sigma}(k_3, k_4+k_5, k_1+k_2) . \quad \text{(B2)}$$

The terms L_j correspond to the diagrams in Fig. 18. The corresponding values, summed over directions of the ghost loops, are given below:

$$\begin{aligned}
&L_1^1 = 27 V^{\alpha\beta\rho}(k_1, k_2, -k_1-k_2) V^{\alpha\beta\sigma}(k_1, k_2, -k_1-k_2) V^{\eta\rho\gamma}(k_4+k_5, k_1+k_2, k_3) V^{\tau\sigma\gamma}(k_4+k_5, k_1+k_2, k_3)(k_5^\eta k_4^\tau + k_4^\eta k_5^\tau),\\
&L_2^1(k_1, k_2, k_3, k_4, k_5) = L_1^1(k_4, k_5, k_3, k_1, k_2),\\
&L_3^1 = 27 V^{\alpha\beta\rho}(k_1, k_2, -k_1-k_2) V^{\alpha\beta\sigma}(k_1, k_2, -k_1-k_2)(k_4\cdot k_5)[(k_4^\rho + k_5^\rho)k_3^\sigma + k_3^\rho(k_4^\sigma + k_5^\sigma)],\\
&L_4^1 = L_3^1,\\
&L_5^1(k_1, k_2, k_3, k_4, k_5) = L_3^1(k_4, k_5, k_3, k_1, k_2),\\
&L_6^1 = L_5^1,\\
&L_7^1 = L_8^1 = L_9^1 = L_{10}^1 = 54(k_1\cdot k_2)(k_4\cdot k_5)(k_1\cdot k_4 + k_1\cdot k_5 + k_2\cdot k_4 + k_2\cdot k_5),\\
&L_{11}^1 = -54(k_1\cdot k_2)[(k_3\cdot k_4)(k_1\cdot k_5 + k_2\cdot k_5) + (k_3\cdot k_5)(k_1\cdot k_4 + k_2\cdot k_4)],\\
&L_{12}^1 = L_{11}^1,\\
&L_{13}^1(k_1, k_2, k_3, k_4, k_5) = L_{11}^1(k_4, k_5, k_3, k_1, k_2),\\
&L_{14}^1 = L_{13}^1,\\
&L_{15}^1 = -27 V^{\eta\rho\gamma}(k_4+k_5, k_1+k_2, k_3) V^{\tau\sigma\gamma}(k_4+k_5, k_1+k_2, k_3)(k_1^\rho k_2^\sigma + k_2^\rho k_1^\sigma)(k_5^\eta k_4^\tau + k_4^\eta k_5^\tau) .
\end{aligned} \quad \text{(B3)}$$

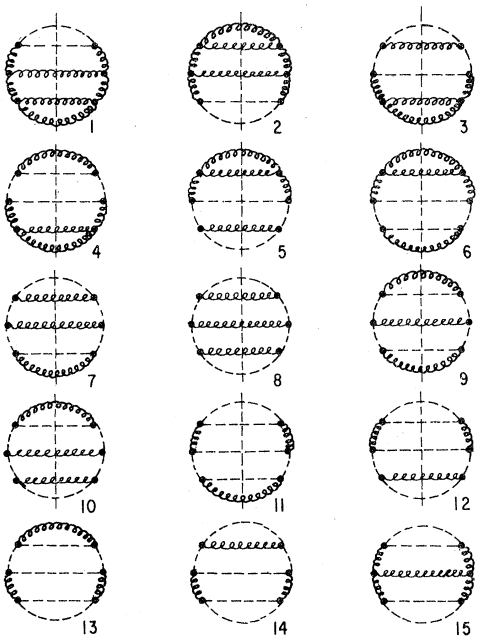

FIG. 18. Complete ghost-loop expansion for $Q_{\rm I}$. Each ghost loop can have two directions.

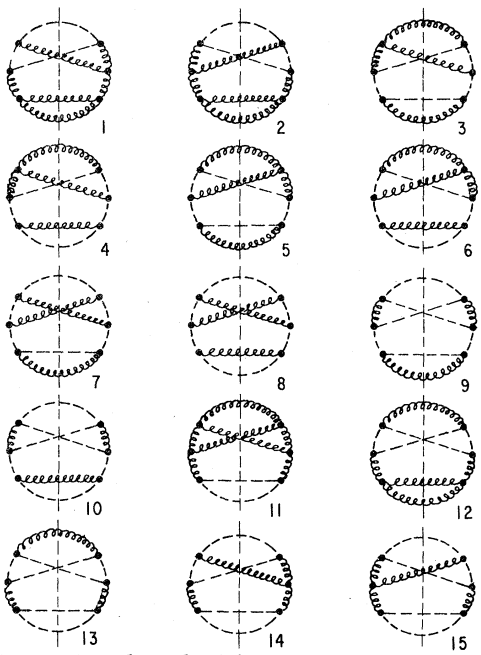

FIG. 19. Complete ghost-loop expansion for $Q_{\rm II}$. Each ghost loop can have two directions.

2. $Q_{\rm II}$

$$4(k_1\cdot k_2)^2(k_4\cdot k_5)(k_3\cdot k_5)Q_{\rm II}=L_0^2-\sum_{j=1}^{12}L_j^2+\sum_{k=13}^{15}L_k^2\,. \tag{B4}$$

The ghostless diagram gives

$$\begin{aligned}L_0^2=&27V^{\alpha\beta\rho}(k_1,k_2,-k_1-k_2)V^{\alpha\beta\sigma}(k_1,k_2,-k_1-k_2)V^{\gamma\eta\rho}(k_3,k_4+k_5,k_1+k_2)\\&\times V^{\delta\sigma\tau}(k_4,k_1+k_2,k_3+k_5)V^{\epsilon\delta\eta}(k_5,k_4,-k_4-k_5)V^{\epsilon\gamma\tau}(k_5,k_3,-k_3-k_5)\,.\end{aligned} \tag{B5}$$

The ghost diagrams in Fig. 19 give

$$\begin{aligned}L_1^2=&-27V^{\alpha\beta\rho}(k_1,k_2,-k_1-k_2)V^{\alpha\beta\sigma}(k_1,k_2,-k_1-k_2)V^{\tau\delta\sigma}(k_3+k_5,k_4,k_1+k_2)[k_3^\rho k_5^\tau(k_4^\delta+k_5^\delta)+(k_4^\rho+k_5^\rho)k_3^\tau k_5^\delta]\,,\\
L_2^2(k_1,k_2,k_3,k_4,k_5)=&L_1^2(k_1,k_2,k_4,k_3,k_5)\,,\\
L_3^2=&27(k_1\cdot k_2)V^{\delta\epsilon\eta}(k_4,k_5,-k_4-k_5)[(k_3^\delta+k_5^\delta)k_3^\epsilon(k_1^\eta+k_2^\eta)+(k_1^\delta+k_2^\delta)(k_3^\epsilon+k_5^\epsilon)k_3^\eta]\,,\\
L_4^2=&L_3^2\,,\\
L_5^2(k_1,k_2,k_3,k_4,k_5)=&L_3^2(k_1,k_2,k_4,k_3,k_5)\,,\\
L_6^2=&L_5^2\,,\\
L_7^2=&54(k_1\cdot k_2)(k_1\cdot k_5+k_2\cdot k_5)(k_3\cdot k_5+k_4\cdot k_5+k_3\cdot k_4)\,,\\
L_8^2=&L_7^2\,,\\
L_9^2=&-54(k_1\cdot k_2)(k_3\cdot k_4)(k_1\cdot k_5+k_2\cdot k_5)\,,\\
L_{10}^2=&L_9^2\,,\\
L_{11}^2=&27V^{\rho\gamma\eta}(k_1+k_2,k_3,k_4+k_5)V^{\sigma\delta\tau}(k_1+k_2,k_4,k_3+k_5)V^{\delta\epsilon\eta}(k_4,k_5,-k_4-k_5)V^{\gamma\epsilon\tau}(k_3,k_5,-k_3-k_5)(k_1^\sigma k_2^\sigma+k_2^\rho k_1^\sigma)\,,\\
L_{12}^2=&-27V^{\alpha\beta\rho}(k_1,k_2,-k_1-k_2)V^{\alpha\beta\sigma}(k_1,k_2,-k_1-k_2)[(k_3\cdot k_5+k_4\cdot k_5+k_3\cdot k_4)k_3^\rho k_4^\sigma+(k_3\cdot k_4)(k_4^\rho+k_5^\rho)(k_3^\sigma+k_5^\sigma)]\,,\\
L_{13}^2=&27\{(k_3\cdot k_5+k_4\cdot k_5+k_3\cdot k_4)[(k_3\cdot k_1)(k_4\cdot k_2)+(k_4\cdot k_1)(k_3\cdot k_2)]\\&+(k_3\cdot k_4)[(k_1\cdot k_4+k_1\cdot k_5)(k_2\cdot k_3+k_2\cdot k_5)+(k_2\cdot k_4+k_2\cdot k_5)(k_1\cdot k_3+k_1\cdot k_5)]\}\,,\\
L_{14}^2=&27V^{\tau\delta\sigma}(k_3+k_5,k_4,k_1+k_2)(k_1^\rho k_2^\sigma+k_2^\rho k_1^\sigma)[k_3^\rho k_5^\tau(k_4^\delta+k_5^\delta)+(k_4^\rho+k_5^\rho)k_3^\tau k_5^\delta]\,,\\
L_{15}^2(k_1,k_2,k_3,k_4,k_5)=&L_{14}^2(k_1,k_2,k_4,k_3,k_5)\,.\end{aligned} \tag{B6}$$

3. $Q_{\rm IV}$

$$8(k_1\cdot k_2)(k_4\cdot k_5)(k_3\cdot k_5)(k_1\cdot k_4)Q_{\rm IV}=L_0^4-\sum_{j=1}^{14}L_j^4+L_{15}^4\,. \tag{B7}$$

The ghostless diagram gives

$$\begin{aligned}L_0^4=&-27V^{\alpha\beta\rho}(k_1,k_2,-k_1-k_2)V^{\rho\gamma\eta}(k_1+k_2,k_3,k_4+k_5)V^{\delta\epsilon\eta}(k_4,k_5,-k_4-k_5)V^{\gamma\epsilon\tau}(k_3,k_5,-k_3-k_5)\\&\times V^{\tau\beta\sigma}(k_3+k_5,k_2,k_1+k_4)V^{\delta\alpha\sigma}(k_4,k_1,-k_4-k_1)\,.\end{aligned} \tag{B8}$$

The ghost contributions corresponding to Fig. 20 are given below.

$$\begin{aligned}L_1^4=&27V^{\alpha\beta\rho}(k_1,k_2,-k_1-k_2)V^{\delta\alpha\sigma}(k_4,k_1,-k_1-k_4)V^{\beta\sigma\tau}(k_2,k_1+k_4,k_3+k_5)[k_3^\tau(k_4^\rho+k_5^\rho)k_5^\delta+k_5^\tau k_3^\rho(k_4^\delta+k_5^\delta)]\,,\\
L_2^4(k_1,k_2,k_3,k_4,k_5)=&L_1^4(k_5,k_3,k_2,k_4,k_1)\,,\\
L_3^4=&-27V^{\alpha\delta\sigma}(k_1,k_4,-k_1-k_4)[(k_1\cdot k_5+k_2\cdot k_5)k_2^\alpha(k_4^\delta+k_5^\delta)(k_3^\sigma+k_5^\sigma)+(k_3\cdot k_4+k_3\cdot k_5+k_4\cdot k_5)(k_1^\alpha+k_2^\alpha)k_5^\delta k_2^\sigma]\,,\\
L_4^4(k_1,k_2,k_3,k_4,k_5)=&L_3^4(k_5,k_3,k_2,k_4,k_1)\,,\end{aligned}$$

$$L_5^4 = 27V^{\alpha\beta\rho}(k_1, k_2, -k_1-k_2)[(k_3\cdot k_4 + k_3\cdot k_5 + k_4\cdot k_5)k_4^\alpha(k_1^\beta + k_4^\beta)k_3^\rho + (k_3\cdot k_4)(k_1^\alpha + k_4^\alpha)(k_3^\beta + k_5^\beta)(k_4^\rho + k_5^\rho)],$$

$$L_6^4(k_1, k_2, k_3, k_4, k_5) = L_5^4(k_5, k_3, k_2, k_4, k_1),$$

$$L_7^4 = 27V^{\tau\sigma\beta}(k_3+k_5, k_1+k_4, k_2)[(k_3\cdot k_4)k_5^\tau k_1^\sigma(k_1^\beta + k_2^\beta) + (k_1\cdot k_5 + k_2\cdot k_5)k_3^\tau k_4^\sigma k_1^\beta],$$

$$L_8^4(k_1, k_2, k_3, k_4, k_5) = L_7^4(k_5, k_3, k_2, k_4, k_1), \tag{B9}$$

$$L_9^4 = -27V^{\epsilon\gamma\tau}(k_5, k_3, -k_3-k_5)V^{\tau\beta\sigma}(k_3+k_5, k_2, k_1+k_4)[(k_4^\epsilon + k_5^\epsilon)(k_1^\gamma + k_2^\gamma)k_1^\beta k_4^\sigma + k_4^\epsilon(k_4^\gamma + k_5^\gamma)(k_1^\beta + k_2^\beta)k_1^\sigma],$$

$$L_{10}^4(k_1, k_2, k_3, k_4, k_5) = L_9^4(k_5, k_3, k_2, k_4, k_1),$$

$$L_{11}^4 = 27[(k_1\cdot k_5 + k_2\cdot k_5)(k_1\cdot k_3 + k_3\cdot k_4)(k_2\cdot k_4) + (k_1\cdot k_2 + k_1\cdot k_4 + k_2\cdot k_4)(k_3\cdot k_4)(k_2\cdot k_5)],$$

$$L_{12}^4(k_1, k_2, k_3, k_4, k_5) = L_{11}^4(k_5, k_3, k_2, k_4, k_1),$$

$$L_{13}^4 = 27[(k_1\cdot k_5)(k_1\cdot k_2 + k_1\cdot k_4 + k_2\cdot k_4)(k_3\cdot k_5 + k_4\cdot k_5 + k_3\cdot k_4) + (k_1\cdot k_4 + k_1\cdot k_5 + k_4\cdot k_5)(k_1\cdot k_5 + k_2\cdot k_5)(k_1\cdot k_3 + k_1\cdot k_5)],$$

$$L_{14}^4 = -27V^{\alpha\delta\sigma}(k_1, k_4, -k_1-k_4)V^{\delta\epsilon\eta}(k_4, k_5, -k_4-k_5)[(k_3^\sigma + k_5^\sigma)k_2^\alpha(k_1^\eta + k_2^\eta)k_3^\epsilon + k_2^\sigma(k_1^\alpha + k_2^\alpha)k_3^\eta(k_3^\epsilon + k_5^\epsilon)],$$

$$L_{15}^4 = 27[(k_1\cdot k_3)(k_2\cdot k_5)(k_1\cdot k_4 + k_1\cdot k_5 + k_4\cdot k_5) + (k_2\cdot k_4 + k_2\cdot k_5)(k_1\cdot k_3 + k_3\cdot k_4)(k_1\cdot k_5) + 2(k_1\cdot k_4 + k_1\cdot k_5)(k_1\cdot k_5 + k_4\cdot k_5)(k_2\cdot k_3)].$$

APPENDIX C: INVARIANT EXPANSIONS

For completeness, we list here invariant expansions for the basic cut diagrams defined in Sec. III.

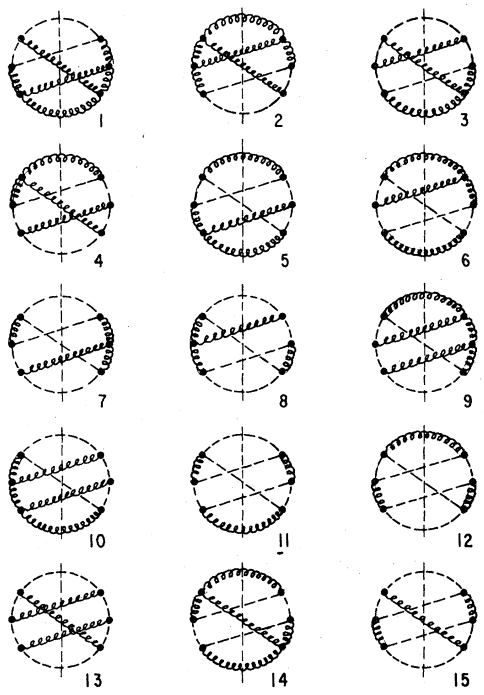

FIG. 20. Complete ghost-loop expansion for Q_{IV}. Each ghost loop can have two directions.

1. Single-gluon processes

The single-gluon traces are defined in Eqs. (3.16) and (3.24). We write these terms as

$$T_J = C_J N_J / D_J . \tag{C1}$$

The coefficients C_J and denominators D_J are given in Table VII. The numerator factors for $T_{\rm I}$, $\tilde{T}_{\rm I}$, and $\tilde{T}_{\rm III}$ are simple:

$$N_{\rm I} = (p_a\cdot p_b)(p_d\cdot p_e) + (p_d\cdot p_a)(p_e\cdot p_b), \tag{C2}$$

$$\tilde{N}_{\rm I} = (p_a\cdot p_b)(p_c\cdot p_d + p_e\cdot p_d)(p_c\cdot p_d + p_c\cdot p_e), \tag{C3}$$

$$\tilde{N}_{\rm III} = (p_d\cdot p_c)(p_b\cdot p_e). \tag{C4}$$

We expand the remaining terms as

TABLE VII. Coefficients and denominators for the expansions of T_J, $\tilde{T}_J$ in Eq. (C1).

Term	C_J	D_J
I	64/3	$(p_b\cdot p_d)^2(p_c\cdot p_e)$
II	28/3	$(p_a\cdot p_e)(p_a\cdot p_c)(p_d\cdot p_e)(p_b\cdot p_d)$
III	8/3	$(p_c\cdot p_e)(p_c\cdot p_a)(p_d\cdot p_e)(p_b\cdot p_d)$
IV	4/3	$(p_b\cdot p_d)^2(p_c\cdot p_e)(p_a\cdot p_e)$
V	12	$(p_b\cdot p_d)^2(p_a\cdot p_c)(p_a\cdot p_e)$
VI	48	$(p_b\cdot p_d)^2(p_a\cdot p_c)^2$
$\tilde{\rm I}$	80/9	$(p_b\cdot p_c)(p_b\cdot p_d)(p_c\cdot p_e)(p_d\cdot p_e)$
$\tilde{\rm II}$	4/9	$(p_b\cdot p_c)(p_b\cdot p_d)(p_a\cdot p_e)(p_c\cdot p_e)$
$\tilde{\rm III}$	64/9	$(p_b\cdot p_c)(p_b\cdot p_d)(p_a\cdot p_e)$
$\tilde{\rm IV}$	4	$(p_a\cdot p_d)(p_b\cdot p_c)(p_b\cdot p_d)(p_c\cdot p_e)$

TABLE VIII. Coefficients C_{ijk} for the sums in Eq. (C5). The scalar products d_j are defined in Eq. (C6). (Throughout these tables, periods indicate zero values.)

tjk	T_{II}	T_{III}	T_{IV}	T_V	T_{VI}	$\tilde{T}_{II}$	$\tilde{T}_{IV}$
111	·	·	·	−1	·	·	−1
112	−1	·	−1	3	1	−1	2
113	1	−1	2	·	·	1	1
114	−3	−1	2	3	·	1	·
115	−1	·	1	2	1	1	1
221	1	·	1	−2	−1	1	−1
222	·	·	·	·	·	·	·
223	·	·	·	·	·	·	·
224	−2	·	·	4	2	·	·
225	−1	·	−1	3	2	−1	1
331	−1	1	−2	1	·	−1	·
332	·	·	·	·	·	·	·
333	·	·	·	·	·	·	·
334	1	−1	2	1	·	1	−1
335	·	·	·	2	2	·	·
441	3	1	−2	−2	·	−1	1
442	−2	·	·	4	2	·	·
443	1	−1	2	2	·	1	−1
444	·	·	·	·	·	·	·
445	·	·	·	·	·	·	·
551	1	·	−1	−1	−1	−1	·
552	−1	·	−1	3	2	−1	1
553	·	·	·	2	2	·	·
554	·	·	·	·	·	·	·
555	·	·	·	·	·	·	·
123	·	3	−1	−1	1	·	−3
124	6	1	−1	−8	−3	·	·
125	2	2	·	−5	−2	·	−3
134	2	6	−4	−4	·	−2	−1
135	·	1	−3	−2	−3	−2	·
145	2	3	−3	−1	1	−2	−1
234	−1	−2	3	4	1	1	−1
235	−1	−1	·	4	2	−1	1
245	−1	−1	·	4	2	−1	1
345	1	−2	1	3	1	1	−1

$$N_J = \sum_{ijk} C_{ijk} d_i d_j d_k , \tag{C5}$$

using the independent dot products

$$\begin{aligned} d_1 &= p_a \cdot p_b , \\ d_2 &= p_a \cdot p_c , \\ d_3 &= p_a \cdot p_d , \\ d_4 &= p_b \cdot p_c , \\ d_5 &= p_b \cdot p_d . \end{aligned} \tag{C6}$$

The required coefficients are listed in Table VIII.

2. Triple-gluon processes

We expand the basic triple-gluon traces of Eq. (3.31) as

$$R_J = C_J N_J / D_J . \tag{C7}$$

TABLE IX. Coefficients and denominators for the expansions of R_J in Eq. (C7).

Term	C_J	D_J
I	512/9	$(p_1\cdot k_1)(p_2\cdot k_3)$
II	64/9	$(p_1\cdot k_1)(p_1\cdot k_2)(p_2\cdot k_3)$
III	4/9	$(p_1\cdot k_1)(p_1\cdot k_3)(p_2\cdot k_3)(p_2\cdot k_2)$
IV	80/9	$(p_1\cdot k_1)(p_1\cdot k_3)(p_2\cdot k_1)(p_2\cdot k_3)$
V	32	$(p_1\cdot k_1)(p_2\cdot k_3)(k_1\cdot k_2)$
VI	2	$(p_1\cdot k_1)(p_1\cdot k_3)(p_2\cdot k_3)(k_1\cdot k_3)$
VII	2	$(p_1\cdot k_1)(p_2\cdot k_3)(p_2\cdot k_2)(k_1\cdot k_3)$
VIII	64	$(k_1\cdot k_2)^2(k_3\cdot p_2)$
IX	8	$(k_1\cdot k_2)^2(p_1\cdot k_3)(p_2\cdot k_3)$
X	9	$(p_1\cdot k_1)(p_2\cdot k_3)(k_1\cdot k_2)(k_2\cdot k_3)$
XI	0	
XII	9	$(p_1\cdot p_2)(p_1\cdot k_1)(p_2\cdot k_3)(k_1\cdot k_2)$
XIII	0	
XIV	36	$(k_2\cdot k_3)^2(p_1\cdot p_2)(p_1\cdot k_1)$
XV	9	$(p_1\cdot p_2)(p_1\cdot k_1)(k_2\cdot k_3)(k_2\cdot k_1)$
XVI	72	$(p_1\cdot p_2)^2(k_2\cdot k_3)^2$
XVII	9	$(p_1\cdot p_2)^2(k_2\cdot k_3)(k_2\cdot k_1)$
XVIII	36	$(p_1\cdot k_1)(p_2\cdot k_3)(p_1\cdot p_2)$
XIX	162	$(p_1\cdot p_2)(k_1\cdot k_2)(p_2\cdot k_3)$
XX	162	$(p_1\cdot p_2)^2(k_1\cdot k_2)$
XXI	1944	$(p_1\cdot p_2)$

The coefficients and denominators are given in Table IX. The color factors for N_{XI} and N_{XIII} vanish. The numerator factors for R_I, R_{II}, R_{IV}, and R_{XXI} are simple:

$$N_I = k_1 \cdot k_3 , \tag{C8}$$

$$N_{II} = (p_1 \cdot k_3)(k_1 \cdot k_2 - p_1 \cdot k_1 - p_1 \cdot k_2) , \tag{C9}$$

$$N_{IV} = (p_1 \cdot p_2)(p_1 \cdot p_2 + p_1 \cdot k_3 - p_2 \cdot k_3) \times (p_1 \cdot p_2 + p_1 \cdot k_1 - p_2 \cdot k_1) , \tag{C10}$$

TABLE X. Coefficients C_{ij} for the sums in Eq. (C12). The scalar products d_j are defined in Eq. (C14).

ij	R_V	R_{VIII}	R_{XVIII}	R_{XIX}	R_{XX}
11	1	1	1	2	−7
22	−2	4	·	·	·
33	·	4	·	·	·
44	·	·	·	·	·
55	·	·	·	·	·
12	·	6	−3	2	−8
13	1	6	−1	2	−8
14	−1	−1	−1	−2	8
15	−1	−1	−1	−2	8
23	·	4	·	·	·
24	1	−4	2	−1	5
25	−2	−2	1	−1	5
34	−1	−2	1	−1	5
35	−2	−4	·	−1	5
45	·	·	·	·	·

TABLE XI. Coefficients C_{ijk} for the sums in Eq. (C13).

ijk	R_{III}	R_{VI}	R_{VII}	R_{IX}	R_{X}	R_{XII}	R_{XIV}	R_{XV}	R_{XVI}	R_{XVII}
111	−1	−5	3	−1	3	−11	8	−6	16	−32
112	.	−4	1	−4	12	−5	8	−21	20	−64
113	−1	−4	3	−4	11	−15	4	−16	8	−33
114	1	9	−4	4	−10	20	−14	17	−20	64
115	.	5	−4	4	−8	12	−4	6	−8	33
221	1	1	−4	−3	5	10	−2	−15	2	−40
222	.	.	.	.	.	.	.	.	.	.
223	.	.	.	.	.	.	.	.	.	.
224	.	.	4	.	2	−8	9	4	17	.
225	−1	3	2	−1	−11	−2	4	1	4	16
331	.	1	.	−3	2	2	4	2	8	5
332	.	.	.	.	.	.	.	.	.	.
333	.	.	.	.	.	.	.	.	.	.
334	.	−1	.	−1	−2	−2	−4	−2	.	−3
335	.	.	.	.	.	.	.	.	.	16
441	.	−4	1	−3	7	−9	6	−11	2	−40
442	.	.	.	.	2	2	−8	−4	−17	.
443	.	.	1	1	13	−7	−2	−15	−4	−16
444	.	.	.	.	.	.	.	.	.	.
445	.	.	.	.	.	.	.	.	.	.
551	1	.	1	−3	5	−1	4	−8	8	5
552	1	−2	1	1	7	−7	−4	−8	.	3
553	.	.	.	.	8	−8	.	−16	.	−16
554	.	.	.	.	.	.	.	.	.	.
555	.	.	.	.	.	.	.	.	.	.
123	1	2	−2	−6	9	4	.	−16	4	−37
124	1	5	−3	5	−10	5	4	24	11	48
125	−1	6	.	3	−19	12	8	10	4	37
134	1	4	−4	3	−24	22	−2	31	4	37
135	1	1	−3	5	−25	17	.	22	.	38
145	1	−4	2	−6	12	−10	2	−15	4	−37
234	1	−3	−2	1	−7	−6	.	5	4	−6
235	.	1	.	1	−10	2	8	.	8	13
245	.	.	3	−1	11	−1	−6	−7	4	6
345	−1	2	3	−1	23	−11	−4	−22	−8	−13

$$N_{XXI} = 1 . \tag{C11}$$

The remaining terms are given by

$$N_J = \sum_{ij} C_{ij} d_i d_j \tag{C12}$$

TABLE XII. Coefficients and denominators for the expansions of Q_J in (C15).

Term	C_J	D_J
I	108	$(k_1\cdot k_2)^2(k_4\cdot k_5)^2$
II	27	$(k_1\cdot k_2)^2(k_4\cdot k_5)(k_3\cdot k_5)$
III	0	
IV	27/2	$(k_1\cdot k_2)(k_1\cdot k_4)(k_3\cdot k_5)(k_4\cdot k_5)$
V	27/4	$(k_1\cdot k_2)(k_1\cdot k_5)(k_4\cdot k_5)$
VI	243/2	$(k_1\cdot k_2)(k_1\cdot k_5)(k_3\cdot k_4)$
VII	1215	$(k_1\cdot k_5)^2(k_3\cdot k_4)$
VIII	29160	$(k_1\cdot k_5)$
IX	1944	$(k_1\cdot k_4)(k_1\cdot k_5)$
X	6561/2	$(k_1\cdot k_5)(k_2\cdot k_4)$

TABLE XIII. Coefficients C_{ij} for the sums in Eq. (C19). The scalar products d_j are defined in Eq. (C21).

ij	Q_V	Q_{VI}	Q_{VII}
11	147	−44	12
22	108	−1	8
33	43	−1	8
44	226	−9	−1
55	44	−9	−1
12	295	−44	16
13	94	−44	16
14	265	−35	10
15	461	−35	10
23	191	−2	16
24	291	−13	6
25	375	−13	6
34	169	−13	6
35	87	−13	6
45	352	−18	−2

TABLE XIV. Coefficients C_{ijk} for the sums in Eq. (C20).

ijk	$Q_{\rm I}$	$Q_{\rm II}$	$Q_{\rm IV}$
111	−170	−196	48
112	−217	−252	−67
113	−88	−252	−175
114	−217	−252	148
115	−88	−252	159
221	−13	−78	−17
222	17	−8	·
223	8	−19	−32
224	119	−56	·
225	24	−57	−15
331	−60	−78	−168
332	8	−19	−127
333	·	−8	−20
334	8	−57	−82
335	·	−56	−28
441	−13	−78	−16
442	119	−56	−64
443	24	−57	13
444	17	−8	·
445	8	−19	15
551	−60	−78	101
552	8	−57	32
553	·	−56	2
554	8	−19	74
555	·	−8	10
123	−28	−280	−321
124	34	−124	−33
125	4	−260	−3
134	4	−260	−29
135	−56	−124	−33
145	−28	−280	209
234	32	−76	13
235	48	−76	−78
245	32	−76	−32
345	48	−76	9

or

$$N_J = \sum_{ijk} C_{ijk} d_i d_j d_k , \tag{C13}$$

with coefficients C_{ij}, C_{ijk} as given in Tables X and XI. The independent scalar products are taken to be

$$\begin{aligned} d_1 &= p_1 \cdot p_2 , \\ d_2 &= p_1 \cdot k_1 , \\ d_3 &= p_1 \cdot k_2 , \\ d_4 &= p_2 \cdot k_1 , \\ d_5 &= p_2 \cdot k_2 . \end{aligned} \tag{C14}$$

3. Five-gluon processes

The five-gluon terms of Eq. (3.36) and Appendix B are written as

$$Q_J = C_J N_J / D_J , \tag{C15}$$

with coefficients and denominators given in Table XII. The color sum for $Q_{\rm III}$ vanishes. The numerator factors for $Q_{\rm VIII}$, $Q_{\rm IX}$ and $Q_{\rm X}$ are

$$N_{\rm VIII} = -1 , \tag{C16}$$

$$N_{\rm IX} = k_1 \cdot k_4 + k_1 \cdot k_5 + 2k_4 \cdot k_5 , \tag{C17}$$

$$N_{\rm X} = k_1 \cdot k_2 + k_1 \cdot k_4 + k_2 \cdot k_5 + k_5 \cdot k_4 . \tag{C18}$$

The remaining terms are expanded as

$$N_J = \sum_{ij} C_{ij} d_i d_j \tag{C19}$$

or

$$N_J = \sum_{ijk} C_{ijk} d_i d_j d_k , \tag{C20}$$

with coefficients C_{ij}, C_{ijk} as given in Tables XIII and XIV. The independent scalar products are taken to be

$$\begin{aligned} d_1 &= k_1 \cdot k_2 , \\ d_2 &= k_1 \cdot k_3 , \\ d_3 &= k_1 \cdot k_4 , \\ d_4 &= k_2 \cdot k_3 , \\ d_5 &= k_2 \cdot k_4 . \end{aligned} \tag{C21}$$

[1]For a discussion of the applicability of QCD perturbation theory see, for example, H. D. Politzer, Phys. Rep. 14C, 129 (1974).

[2]A thorough review of QCD can be found in W. Marciano and H. Pagels, Phys. Rep. 36C, 137 (1978).

[3]H. D. Politzer, Nucl. Phys. B129, 309 (1977); S. Libby and G. Sterman, Phys. Lett. 78B, 618 (1978); R. K. Ellis, H. Georgi, M. Machacek, H. D. Politzer, and G. G. Ross, *ibid.* 78B, 281 (1978); Nucl. Phys. B152, 285 (1979).

[4]C. T. Sachrajda, Phys. Lett. 73B, 185 (1978); W. Furmanski, Jagellonion University Report No. TPJU 10/78, 1978 (unpublished); Phys. Lett. 77B, 312 (1978).

[5]A. Mueller, Phys. Rev. D 18, 3705 (1978); D. Amati, R. Petronzio, and G. Veneziano, Nucl. Phys. B140, 54 (1978).

[6]See, for example, the speculation of J. Ellis, M. K. Gaillard, and W. J. Zakrewski, Phys. Lett. 81B, 224 (1979).

[7]Some pessimistic early conclusions drawn from higher-order calculations were reported by R. Feynman at the

1979 Caltech workshop on High Energy Physics (unpublished).
[8]R. D. Field, Phys. Rev. Lett. 40, 997 (1978); R. P. Feynman, R. D. Field, and G. C. Fox, Phys. Rev. D 18, 3320 (1978).
[9]J. F. Owens, E. Reya, and M. Gluck, Phys. Rev. D 18, 1501 (1978); J. F. Owens and J. D. Kimel, *ibid.* 18, 3313 (1978); J. F. Owens, FSU Report No. FSU-HEP-781220, 1978 (unpublished).
[10]A. P. Contogouris, R. Gaskell, and S. Papadopoulos, Phys. Rev. D 17, 2314 (1978).
[11]R. Blankenbecler, S. J. Brodsky, and J. F. Gunion, Phys. Rev. D 18, 900 (1978); D. Jones and J. F. Gunion, *ibid.* 19, 867 (1978).
[12]E. G. Floratos, D. A. Ross, and C. T. Sachrajda, Nucl. Phys. B129, 66 (1977); B139, 545 (1978).
[13]W. A. Bardeen, A. J. Buras, D. W. Duke, and T. Muta, Phys. Rev. D 18, 3998 (1978).
[14]J. Ellis, M. K. Gaillard, and G. G. Ross, Nucl. Phys. B111, 253 (1976); A. De Rújula, J. Ellis, E. G. Floratos, and M. K. Gaillard, *ibid.* B138, 387 (1978).
[15]C. L. Basham, L. S. Brown, S. D. Ellis, and S. T. Love, Phys. Rev. D 17, 2298 (1978); Phys. Rev. Lett. 41, 1585 (1978).
[16]G. C. Fox and S. Wolfram, Phys. Rev. Lett. 41, 1581 (1978); Nucl. Phys. B149, 413 (1978).
[17]G. Sterman and S. Weinberg, Phys. Rev. Lett. 39, 1436 (1977); P. M. Stevenson, Phys. Lett. 78B, 451 (1978).
[18]B. L. Combridge, Phys. Rev. D 18, 734 (1978).
[19]J. Kripfganz and A. Schiller, Phys. Lett. 79B, 317 (1978); A. Schiller, J. Phys. G 5, 1329 (1979).
[20]C. J. Maxwell, Nucl. Phys. B149, 61 (1979).
[21]G. Sterman, Phys. Rev. D 17, 2773 (1978); 17, 2789 (1978).
[22]G. Tiktopoulos, Nucl. Phys. B147, 371 (1979).
[23]W. Furmanski, Jagellonian Report No. TPJU-11/78 (unpublished).
[24]J. D. Bjorken, Phys. Rev. D 8, 4098 (1973).
[25]See, for example, D. Sivers, S. Brodsky, and R. Blankenbecler, Phys. Rep. 23C, 1 (1977), and references therein.
[26]S. Brodsky and G. Farrar, Phys. Rev. Lett. 3, 1153 (1973); V. Matveev, R. Muradyn, and A. Tavkhelidze, Lett. Nuovo Cimento 7, 719 (1973).
[27]W. E. Caswell, R. R. Horgan, and S. J. Brodsky, Phys. Rev. D 18, 2415 (1978); R. R. Horgan and P. N. Scharbada, Phys. Lett. 81B, 215 (1979).
[28]E. Farhi, Phys. Rev. Lett. 39, 1587 (1977).
[29]J. Bjorken and S. Drell, *Relativistic Quantum Mechanics* (McGraw-Hill, New York, 1965).
[30]R. Cutler and D. Sivers, Phys. Rev. D 17, 196 (1978).
[31]R. P. Feynman, Acta Phys. Pol. 24, 297 (1962); L. D. Faddeev and V. N. Popov, Phys. Lett. 25B, 29 (1967).
[32]G. Altarelli and G. Parisi, Nucl. Phys. B126, 298 (1977).
[33]C. S. Lam and T. M. Yan, Phys. Lett. 71B, 173 (1977).
[34]K. Schilcher, Phys. Rev. D 19, 796 (1979).